Ogawa, Lim et al.

1 Antibody-directed extracellular proximity biotinylation reveals Contactin-1 regulates axo-

2 axonic innervation of axon initial segments.

3

4 Yuki Ogawa[1†], Brian C. Lim[1†], Shanu George[2], Juan A. Oses-Prieto[3], Joshua M. Rasband[1], Yael

5 Eshed-Eisenbach[4], Supna Nair[3], Francesco Boato[2], Elior Peles[4], Alma L. Burlingame[3] Linda Van

6 Aelst[2], and Matthew N. Rasband[1]

7

8 [1] Baylor College of Medicine, Department of Neuroscience, Houston, TX, USA
9 [2]Cold Spring Harbor Laboratory, Division of Neuroscience, Cold Spring Harbor, NY, USA
10 [3] University of California San Francisco, Department of Pharmaceutical Chemistry, San
11 Francisco, CA, USA
12 [4]Weizmann Institute of Science, Department of Molecular Cell Biology, Rehovot, Israel.
13
14 [†] These authors contributed equally to this work.
15
16 Address correspondence to:
17
18 Dr. Matthew N. Rasband
19 Department of Neuroscience
20 Baylor College of Medicine
21 One Baylor Plaza
22 Houston, TX, 77030
23
24 rasband@bcm.edu
25 Tel: 713-798-4494
26
27 8 figures, 5 supplemental figures, 3 supplemental tables, 1 supplemental data files.

Ogawa, Lim et al.

28 **ABSTRACT**

29   Axon initial segment (AIS) cell surface proteins mediate key biological processes in

30 neurons including action potential initiation and axo-axonic synapse formation. However, few

31 AIS cell surface proteins have been identified. Here, we used antibody-directed proximity

32 biotinylation to define the cell surface proteins in close proximity to the AIS cell adhesion

33 molecule Neurofascin. To determine the distributions of the identified proteins, we used

34 CRISPR-mediated genome editing for insertion of epitope tags in the endogenous proteins. We

35 found Contactin-1 (Cntn1) among the previously unknown AIS proteins we identified. Cntn1 is

36 enriched at the AIS through interactions with Neurofascin and NrCAM. We further show that

37 Cntn1 contributes to assembly of the AIS-extracellular matrix, and is required for AIS axo-axonic

38 innervation by inhibitory basket cells in the cerebellum and inhibitory chandelier cells in the

39 cortex.

40

Ogawa, Lim et al.

41 **MAIN**

42   The axon initial segment (AIS) is essential for proper neuronal and brain circuit function.

43 AIS integrate synaptic inputs, generate and modulate axonal action potentials, and regulate the

44 trafficking of proteins, vesicles, and organelles to maintain neuronal polarity. These functions

45 depend on a tightly regulated network of scaffolding and cytoskeletal proteins that serve as an

46 organizing platform for ion channels and cell adhesion molecules (CAMs) [1,2]. However, the AIS

47 proteins that have been described likely represent only a small fraction of the overall AIS

48 proteome since the molecular mechanisms involved in many AIS-associated processes remain

49 poorly defined.

50   Recently, proximity-dependent biotinylation (PDB) approaches have emerged as robust

51 experimental strategies to define the molecular composition of organelles and subcellular

52 domains [3]. PDB is particularly attractive to identify AIS proteomes since the AIS is very

53 detergent insoluble and refractory to more traditional proteomic approaches like

54 immunoprecipitation (IP) mass-spectrometry. Streptavidin pulldown of biotinylated AIS

55 proteins allows for the use of much stronger solubilizing detergents. We previously used one

56 PDB approach (BioID) to discover new AIS proteins [4]; we targeted the biotin ligase BirA* to the

57 AIS by fusing it to a variety of known AIS cytoskeleton-associated proteins. These experiments

58 identified known and some new cytoplasmic AIS proteins, including Mical3 and Septins.

59 However, our experiments were strongly biased towards cytoplasmic proteins and recovered

60 very few membrane and cell surface proteins. Some PDB approaches have successfully

61 captured cell surface proteins. For example, Li et al. (2020) [5] used an extracellular, membrane

62 tethered horseradish peroxidase (HRP) to identify cell surface proteins that function as

3

63 regulators of neuronal wiring; their transgenic approach revealed the cell surface proteome of

64 *Drosophila* olfactory projection neurons. Shuster et al. [6] used the same approach in mice, but

65 restricted the expression of the membrane tethered HRP to Purkinje neurons to reveal their cell

66 surface proteome. However, neither of these approaches was designed to interrogate

67 subcellular domains. As an alternative approach, Takano et al. (2020) [7] used a split PDB

68 strategy (Split-TurboID) to elucidate the cell surface proteome of astrocyte-neuron synapses.

69 Their experiments revealed transcellular interactions between neuronal NrCAM and astrocytic

70 NrCAM that stabilize the structure and function of inhibitory synapses.

71   To overcome some of the limitations of intracellular PDB for identification of AIS cell

72 surface proteins, we used Selective Proteomic Proximity Labeling Assay Using Tyramide

73 (SPPLAT) [8,9]; the approach has also been called Biotinylation by Antibody Recognition (BAR) [10].

74 Our application of this strategy uses highly specific primary antibodies against the extracellular

75 domain of the AIS-enriched CAM Neurofascin (Nfasc) to direct HRP conjugated secondary

76 antibodies to the AIS. Addition of biotin-tyramide and hydrogen peroxide generates biotin

77 phenoxyl radicals that biotinylate membrane proteins within a range of ~250 nanometers of the

78 peroxidase [11]. We performed this labeling at multiple timepoints throughout neuronal

79 development *in vitro* on live neurons. We identified all previously reported AIS extracellular,

80 and membrane cell adhesion and recognition molecules. In addition, we found many novel

81 membrane proteins that were reproducibly in proximity to Nfasc, with different temporal

82 enrichment profiles. We further investigated a subset of these using CRISPR-mediated

83 endogenous gene tagging. Among these, we identified Contactin-1 (Cntn1) as a new, *bona fide*

84 AIS CAM recruited to the AIS through interaction with the AIS CAMs Nfasc and NrCAM.

85   Remarkably, loss of Cntn1 severely impaired inhibitory axo-axonic innervation of the AIS in both

86   cerebellar Purkinje neurons and cortical pyramidal neurons. Thus, using antibody directed

87   extracellular proximity biotinylation, we identified Cntn1 as a new AIS protein that regulates

88   axo-axonic innervation of the AIS.

89

90   ***Proximity Biotinylation at the AIS Membrane***

91   We reasoned the Nfasc proximity proteome could be used to help define the AIS cell

92   surface proteome since Nfasc is highly enriched at the AIS. Therefore, we adapted the

93   SPPLAT/BAR method [8,10] for use with live, unpermeabilized neurons; we avoided fixation to

94   maximize protein recovery and subsequent mass spectrometry. We labeled rat hippocampal

95   neurons in culture with highly specific and validated chicken primary antibodies against the

96   ectodomain of Nfasc [12], since its 186 kDa isoform (NF186) is highly enriched at the AIS (Fig. 1a,

97   b), with lower concentrations along the distal axon, at growth cones, and in the soma [13]. After

98   live labeling with the anti-Nfasc primary antibody, HRP-conjugated anti-chicken secondary

99   antibodies were used to label the anti-Nfasc primary antibody. The Nfasc-localized HRP

100   generates the reactive biotin phenoxyl from biotin tyramide (biotin phenol), resulting in the

101   addition of tyrosine residues to proteins in proximity to Nfasc with a range of several hundred

102   nm [9,11]. As with other PDB methods, nonspecifically and endogenously biotinylated proteins, as

103   well as non-specific protein background adsorbing to solid phase surfaces during the

104   enrichment steps and prior to the mass spectrometry analysis, must be excluded. The omission

105   of the primary antibody serves as a simple and straightforward negative control. Without

106   fixation or detergents, the membrane-impermeability of biotin-phenoxyl restricts the

5

Ogawa, Lim et al.

107   biotinylation reaction to the extracellular surface. Hereafter, we refer to this method as Nfasc-

108   BAR.

109   We found that Nfasc-BAR resulted in AIS-enriched streptavidin labeling that colocalized

110   with NF186 (Fig. 1b); this pattern was not seen when the anti-Nfasc antibody was omitted. The

111   amount of biotinylation also depends on the duration of the labeling reaction (Fig. S1a). For the

112   experiments described below, we used a reaction time of 5 minutes (Fig. S1b). To identify

113   biotinylated AIS proteins, we then solubilized neuronal membranes using a strong solubilization

114   buffer, purified biotinylated proteins using streptavidin-conjugated magnetic beads, and finally

115   identified the biotinylated proteins using mass spectrometry (Fig. 1a). To confirm the

116   reproducibility and robustness of our approach we performed surface proximity labeling in

117   parallel using rabbit polyclonal antibodies targeting the ectodomain of NrCAM (Fig. S1c),

118   another AnkG-binding CAM found at the AIS. Proximity biotinylation directed by NrCAM

119   antibodies strongly labeled the AIS (Fig. S1c). Importantly, the resulting mass spectrometry

120   datasets confirmed the robustness of the strategy since Nfasc-BAR and NrCAM-BAR proximity

121   proteomes were highly concordant (Fig. S1d; supplemental Table 1).

122

123   ***NF186 proximity proteomes across neuronal development***

124   The maturation of axons includes the enrichment of proteins that mediate key functions

125   or developmental mechanisms. For example, toward the end of the first week *in vitro*, the

126   scaffolding protein AnkyrinG (AnkG) localizes to the proximal axon; this enrichment precedes

127   and is necessary for the subsequent recruitment of Nfasc, and voltage-gated Na$^+$ (Nav) and K$^+$

128   (Kv) channels to the AIS [14,15]. NF186 enrichment at the AIS and along distal axons also increases

6

Ogawa, Lim et al.

129   during development (Fig. 2a). To determine the extracellular Nfasc proximity proteome and

130   how it changes during development (both before and after AIS formation), we performed

131   Nfasc-BAR on primary hippocampal neurons at five different timepoints (supplemental Table 2):

132   from day *in vitro* 4 (DIV4; prior to AIS formation) to DIV28 after establishment of the AIS-

133   associated ECM (Fig. S2); all experiments were performed three times independently for each

134   developmental timepoint with 2 million neurons per experiment. To compare Nfasc cell surface

135   proximity proteomes from cultures of different ages, we normalized peptide spectral match

136   (PSM) counts to total spectral counts in the set of endogenously biotinylated carboxylases

137   detected (Fig. S2), as a correction factor for differences in total protein amount used in

138   individual pulldowns (see methods). We found that as neurons, the AIS, and axons develop, the

139   cell surface Nfasc proximity-proteome changes, with an increasing number of proteins

140   displaying significant changes in fold enrichment (Fig. 2, supplemental Table 2). Consistent with

141   a developing and maturing AIS and increasing levels of overall Nfasc, volcano plots (Fig. 2a and

142   supplemental table 3) show the enrichment of proteins identified using Nfasc-BAR compared to

143   controls at the various developmental time points. We used a cutoff of $\log_2$(Nfasc PSMs/Ctrl

144   PSMs) or $\log_2$[fold change (FC)] >2 (vertical dotted line) with a significance cutoff of $p<0.05$

145   (horizontal dotted line).

146   To visualize the increase in proteins identified using Nfasc-BAR across development and

147   to select candidates to focus on, we identified 285 proteins that satisfied two filtering criteria

148   for at least one of the five timepoints: (1) normalized PSMs > 10 and (2) $\log_2$(Nfasc PSMs/Ctrl

149   PSMs) or $\log_2$(FC) > 2 (Fig. S2; Supplemental Table 2). Among these 285 proteins there were a

150   variety of protein expression profiles (Fig. 2b). Although present, relatively few proteins

Ogawa, Lim et al.

151 showed a reduction in the cell surface Nfasc proximity proteome. Most proteins identified in

152 the Nfasc proximity proteome increased in abundance (Fig. 2c; only the 100 candidates with the

153 largest increase across all time points are shown). We also plotted the log$_2$FC at each time

154 point for the 100 proteins with the largest fold change (DIV 4 only had 63 proteins with log$_2$FC

155 >2) (Fig. S3). The results for each protein were highly reproducible at each time point and

156 consistently revealed similar sets of cell surface proteins. Cytoplasmic AIS proteins such as

157 AnkG, β4 spectrin, and TRIM46 were conspicuously absent consistent with our experimental

158 design to restrict the biotinylation to cell surface proteins.

159

160 ***The Nfasc-BAR proximity proteome includes AIS enriched proteins***

161   Among the cell surface proteins that passed our selection criteria (Fig. S2), we found all

162 known AIS membrane proteins and AIS enriched extracellular matrix molecules with the

163 notable exception of ion channels (Fig. 3a). Why might that be the case since ion channels are

164 known to be highly enriched at the AIS? The number of PSMs recovered for any protein

165 depends on: 1) the number of available extracellular tyrosine residues (Nfasc-BAR-mediated

166 biotinylation occurs on tyrosine residues); 2) the amount and local membrane density of the

167 protein; and 3) the proximity of the protein to the biotinylation source. Since ion channels are

168 highly enriched at the AIS and are in close proximity to Nfasc, their absence from our data set

169 likely reflects the small number of extracellular tyrosine residues found in ion channels and a

170 topology that has extracellular residues very close to the membrane. For example, the AIS-

171 enriched K$^+$ channel subunit KCNQ3 has four extracellular regions comprising 45 amino acids,

172 with two of those being tyrosine (Fig. 3b); we did not detect any KCNQ3 peptides in our

8

Ogawa, Lim et al.

173   experiments. Similarly, Nav1.2 (encoded by *Scn2a*), the main voltage-gated Na$^+$ channel

174   expressed at AIS in DIV14 hippocampal neurons, has an average of one tyrosine per

175   extracellular domain and many are very close to or immediately adjacent to the membrane.   In

176   contrast to ion channels, cell adhesion molecules like Nfasc and Contactin-1 (Cntn1) have large

177   extracellular domains with many tyrosine residues (Fig. 3b). Thus, the low number of

178   extracellular tyrosines found in ion channels and the proximity of these residues to the

179   membrane may make them difficult to biotinylate using Nfasc-BAR; other membrane or cell

180   surface proteins with few or inaccessible tyrosine residues may also be poorly represented in

181   our data set.

182   In contrast to ion channels, an analysis of the 201 proteins identified at DIV14 showed

183   no correlation between the number of PSMs for a protein and the number of extracellular

184   tyrosines (Figs. 3c, d). This suggests a much stronger dependence of PSM number on proximity

185   and protein abundance. As an estimate for both proximity and abundance, we calculated the

186   ratio of extracellular tyrosines to PSM count for all 201 proteins identified at DIV14. Thus, a

187   lower ratio suggests greater abundance of protein and closer proximity to the HRP-dependent

188   biotinylation source (Fig. 3e). This analysis shows many candidates with low extracellular

189   tyrosine/PSM ratios that were also previously reported to be directly or indirectly linked to

190   Nfasc, including PlxnA4, Ncam1, L1CAM, and NrCAM (Fig. 3e) [16,17].

191

192   ***Tagging of endogenous membrane proteins***

193   Our results across 5 developmental timepoints yielded an NF186 proximity proteome

194   (Fig. 2a); filtering based on fold-enrichment and number of PSMs recovered resulted in 285

9

195   candidate cell surface proteins in close proximity to NF186 (Fig. S2). Among these, Nfasc-BAR

196   successfully identified the 13 previously reported AIS-enriched cell surface proteins (excluding

197   ion channels; Fig. 3a). However, it is unlikely that the remaining 272 proteins are also enriched

198   at the AIS since NF186 is present in lower densities in the soma, axons, and at growth cones [13],

199   some of the proteins were identified before the AIS forms or is mature (e.g., DIV4), and the

200   range of SPPLAT/BAR is ~200-300 nm [9,11]. Thus, proteins identified by Nfasc-BAR may be in

201   proximity to NF186 but not enriched at the AIS. We previously used antibodies to validate the

202   AIS proteomes we identified using BioID [4]. However, antibodies are frequently non-specific and

203   for reasons that are unclear, many antibodies that label AIS are not against their claimed

204   targets [18-20]. Therefore, to circumvent some of the challenges associated with antibodies and to

205   look for AIS- and axon-enriched proteins, we performed CRISPR-mediated epitope tagging of

206   endogenous proteins [19,21-23]. We selected 23 different candidates (Fig. 4a) identified using

207   Nfasc-BAR based on 1) the high fold-enrichment compared to control BAR, 2) the high number

208   of PSMs recovered, and 3) the estimate of proximity to the biotin source (Figs. 2 and 3).

209   Included in these 23 candidates were four cell adhesion molecules previously reported at the

210   AIS: Nfasc, NrCAM, L1CAM, and Cntn2 [24-26]. To endogenously label these 23 cell surface

211   proteins, we generated two adeno-associated viruses (AAV) to transduce cultured DIV 0 rat

212   hippocampal neurons with 1) Cas9 and 2) a gene specific single guide RNA (sgRNA), a sgRNA

213   that recognizes donor recognition sites (DRS) flanking spaghetti monster fluorescent protein

214   with V5 tags (smFP-V5), and smFP-V5 (Fig. 4b). The gene specific sgRNAs were targeted to the

215   last exon of each gene of interest allowing for the insertion of smFP-V5 in the last exon. 2

216   weeks after transduction, neurons were fixed and immunostained for β4 spectrin to label the

Ogawa, Lim et al.

217   AIS, and V5 to detect the endogenously tagged cell surface protein. Since we targeted the last

218   exon (C-terminus) of each protein resulting in premature termination of the protein, it is

219   possible the addition of the smFP-V5 disrupted the normal localization of the cell surface

220   protein. However, C-terminal tagging of endogenous Nfasc, NrCAM, L1CAM, and Cntn2 all

221   resulted in AIS labeling as previously reported [25-27] (Figs. 4c-f). The candidates we tested

222   labeled AIS, axons, and dendrites (Figs. 4 and S4). For example, endogenous tagging of Ncam1

223   revealed uniform surface labeling in somatodendritic, AIS, and axonal domains (Fig. 4g), while

224   Ptprs and Tenm4 showed preferential labeling of AIS and axons (Figs. 4h, i); endogenous

225   labeling of Adgrl3 strongly labeled dendrites and spines (Fig. 4j). Among all the candidates we

226   tested that had not previously been reported at the AIS, we found that endogenous tagging of

227   Cntn1 showed the strongest labeling at the AIS (Fig. 4k).

228

229   ***Cntn1 is a bona fide AIS cell surface protein***

230   Cntn1 is a glycosylphosphatidyl inositol (GPI)-anchored cell adhesion molecule widely

231   expressed throughout the nervous system in both neurons and glia [28]. It has essential roles in

232   forming the axoglial junctions flanking nodes of Ranvier where it forms a complex together with

233   axonal Caspr and the glial 155 KDa splice variant of Nfasc (NF155) [29,30]. Cntn1-null mice die in

234   the 3rd postnatal week, emphasizing the importance of Cntn1 to normal function. Cntn1 was

235   also reported at nodes of Ranvier, although its function there is unknown [31]; detection of nodal

236   or paranodal Cntn1 requires different fixation and treatment conditions [32], suggesting that in

237   some subcellular domains Cntn1 may engage in protein-protein interactions that preclude

238   immunostaining. With this in mind, our efforts to immunolabel Cntn1 at AIS in control mouse

11

Ogawa, Lim et al.

239   brain failed. Nevertheless, we performed immunostaining *in vitro* using a goat-polyclonal anti-

240   Cntn1 antibody in control and Cntn1-deficient neurons. We disrupted endogenous Cntn1

241   expression in cultured hippocampal neurons using AAV to express Cas9 and three control or

242   three *Cntn1* specific sgRNAs (Fig. 5a). Whereas neurons transduced with Cas9 and the control

243   sgRNAs had Cntn1 and AnkG immunolabeling at the AIS (Fig. 5b, arrowheads), neurons

244   transduced with the *Cntn1* sgRNAs lost both the perisomatic and AIS Cntn1 immunoreactivity

245   (Fig. 5c, arrowhead). Thus, immunostaining of cultured hippocampal neurons reveals AIS

246   Cntn1. These results also demonstrate the specificity of the Cntn1 antibody. However, loss of

247   AIS Cntn1 had no effect on AIS AnkG (Fig. 5c, arrowhead), or clustering of Nfasc or Na$^+$ channels

248   (data not shown).

249   Transduction of DIV10 cultured hippocampal neurons using AAV to express myc-tagged

250   Cntn1 (Fig. 5d, e) also showed Cntn1-myc enriched at the AIS that colocalized with β4 spectrin

251   at DIV14 (Fig. 5e, arrowheads). Similarly, retro-orbital injection of AAV Cntn1-myc in 13-week

252   old mice, showed strong AIS enrichment of Cntn1-myc in transduced cortical neurons four

253   weeks after injection (Fig. 5d, f, arrowheads). Finally, we performed *in vivo* AAV-dependent and

254   CRISPR-mediated tagging of endogenous Cntn1 using smFP-V5 (Fig. 5g). As with cultured

255   neurons (Fig. 4k), we found the sgRNA targeting *Cntn1* resulted in V5 labeling of cortical neuron

256   AISs (Fig. 5h, arrowheads). Together, these results show that Cntn1 is a *bona fide* AIS cell

257   surface protein.

258

259   ***Cntn1 is localized at the AIS through binding to L1-family cell adhesion molecules***

12

260   Since Cntn1 is a GPI-anchored cell surface protein, we reasoned that it must be

261   recruited to the AIS through interactions with a co-receptor or some other AIS transmembrane

262   protein. Cntn1 has 6 N-terminal immunoglobulin-like (Ig-like) and 4 C-terminal fibronectin III

263   (FNIII) domains (Fig. 6a). To determine how Cntn1 is clustered at the AIS, we generated myc-

264   tagged Cntn1 with various internal deletions of these domains. We found the N-terminus and

265   first four Ig-like domains of Cntn1 are required for its AIS clustering (Fig. 6b). In contrast,

266   deletion of the last two Ig domains or any of the FNIII domains did not affect recruitment of

267   Cntn1 to the AIS (Fig. 6c).

268   What membrane protein recruits Cntn1 to the AIS? Biochemical and cell biological

269   studies suggest that Cntn1 interacts with members of the AnkG-binding L1 family of cell

270   adhesion molecules including Nfasc, L1CAM, and NrCAM [33,34]. Although all three of these CAMs

271   are enriched at the AIS, L1CAM is also found at high levels along the distal axon (Figs. 4c-e). To

272   determine if the AIS-enriched Nfasc or NrCAM recruits Cntn1 to the AIS, we generated sgRNAs

273   vectors (Fig. 5a) to delete Nfasc and NrCAM from neurons. Surprisingly, removal of Nfasc or

274   NrCAM alone had no effect on the clustering of Cntn1 at the AIS (Figs. 6d, e). However,

275   simultaneous deletion of both Nfasc and NrCAM blocked the AIS clustering of Cntn1 (Figs. 6d,

276   arrowhead; e).   These results suggest that the AIS enriched CAMs Nfasc and NrCAM

277   redundantly recruit Cntn1 to the AIS through its first four Ig-like domains.

278

279   **Cntn1 helps assemble the AIS extracellular matrix**

280   We found Tenascin-R (Tnr) in our Nfasc-BAR proximity proteome (Fig. 3a). Tnr is an

281   extracellular matrix molecule and a known Cntn1 interactor [33].   Immunostaining of cultured

Ogawa, Lim et al.

282   hippocampal neurons using antibodies against Tnr showed that it strongly labeled the AIS and

283   colocalizes with Nfasc (Fig. 6f). Previous studies showed that Nfasc regulates the AIS

284   recruitment of the extracellular matrix molecule Brevican [15]. To determine if Nfasc or Cntn1

285   also regulate the AIS clustering of extracellular Tnr, we disrupted expression of *Nfasc* and

286   *Cntn1*; sgRNA vectors (Fig. 5a) targeting *Nfasc* and *Cntn1* were highly efficient (Figs. 5c and 6g).

287   Although control sgRNAs had no effect on AIS Tnr, loss of both Nfasc and Cntn1 significantly

288   reduced Tnr's AIS enrichment (Fig. 6g, h). Thus, Nfasc and Cntn1 both contribute to the

289   assembly or stabilization of the Tnr-containing AIS extracellular matrix.

290

291   ***Cntn1 regulates the assembly of pinceau synapses in the cerebellum.***

292   Purkinje neuron AISs are innervated by inhibitory basket cell interneurons that

293   powerfully modulate neuronal excitability [35]. Basket cells form a stereotypical 'pinceau'

294   synapse (Fig. 7a), with presynaptic terminals at the AIS highly enriched in Kv1 K$^+$ channels and

295   PSD-95, among other proteins [36]. The loss of the AIS scaffolding protein AnkG disrupts pinceau

296   synapses and the AIS clustering of Nfasc, suggesting that their assembly requires AnkG-

297   dependent clustering of CAMs like Nfasc and NrCAM [37]. Since AIS enrichment of Cntn1 also

298   depends on these CAMs, we wondered if Cntn1 plays important roles in cerebellar pinceau

299   synapse assembly. Therefore, we examined pinceau synapse formation in P18 *Cntn1 -/-* mice;

300   *Cntn1 -/-* are very sick and typically die before 3 weeks of age [30]. Immunostaining of Purkinje

301   neurons using antibodies against Nfasc, Kv1.2, and PSD95 showed stereotypical enrichment and

302   clustering of these proteins at the AIS of control heterozygote *Cntn1 -/+* mice, but *Cntn1 -/-*

303   mice had profoundly disrupted pinceau synapse formation (Fig. 7b, arrows) with significantly

14

Ogawa, Lim et al.

304 reduced Kv1.2 and PSD95 intensity at the pinceau synapse (Fig. 7c). Thus, Cntn1 is required for

305 proper assembly of pinceau synapses at the AIS of cerebellar Purkinje neurons.

306

307 ***Cntn1 regulates axo-axonic innervation of pyramidal neurons by chandelier cells***

308 In the cortex and hippocampus, axo-axonic synapses are formed between chandelier

309 cells (ChCs, also known as axo-axonic cells) and the AIS of pyramidal neurons (PyNs). ChCs are

310 derived from progenitors in the ventral region of the medial ganglionic eminence. They have a

311 unique axonal arbor consisting of multiple arrays of short, vertically oriented terminals of

312 presynaptic boutons called cartridges, and each of these cartridges selectively innervates

313 neighboring PyN AISs. These ChCs powerfully reduce PyN output by inhibiting AIS excitability;

314 this inhibition can subsequently modulate brain circuit function and behavior [38-40]. However,

315 the mechanisms that control the precise innervation of PyN AISs by ChCs remains incompletely

316 understood, with ankyrin-interacting L1CAM so far being the only CAM known to be required

317 for ChC/PyN AIS innervation [41]; since L1CAM is found throughout the axon and not just at the

318 AIS, additional mechanisms must exist to allow for precise AIS innervation. To determine if

319 Cntn1 regulates ChC/PyN AIS innervation, we performed in utero electroporation (IUE) using

320 control or *Cntn1*-targeting sgRNA- and smFP-HA-expressing plasmids in *Nkx2.1-CreER;Rosa26-*

321 *loxpSTOPloxp-tdTomato (Ai9)* pregnant mice at embryonic day 15.5 (E15.5) (Fig. 8a). This

322 timing of IUE results in disruption of the *Cntn1* gene in layer II/III PyNs. At E18.5 tamoxifen was

323 administered to the pregnant mother to induce expression of tdTomato red fluorescence

324 protein (RFP) in a sparse group of layer II ChCs (Fig. 8b). We collected brains from P17 mice and

325 analyzed the innervation and assembly of inhibitory synapses on PyN AISs by immunostaining

326   for AnkG or β4 spectrin to label AISs, and antibodies to gephyrin and VGAT to label post- and

327   pre-synaptic compartments of GABAergic synapses, respectively. We found that transfection

328   with Cntn1 sgRNA significantly reduced the percentage of PyN AISs innervated by single RFP-

329   positive ChCs in layer II/III of the somatosensory cortex, as compared to control sgRNA (Figs. 8c,

330   arrowheads, and d). We found that Cntn1-deficient neurons also had significantly fewer

331   inhibitory synapses along their AIS as indicated by gephyrin (Figs. 8e and f) and VGAT puncta

332   (Figs. 8g and h). Together, these results show that Cntn1 is required for efficient ChC/PyN AIS

333   innervation and consequently, the proper assembly of AIS axo-axonic inhibitory synapses.

334

335   **DISCUSSION**

336   AIS properties essential for brain function include: 1) high densities of ion channels, 2)

337   mechanisms to regulate neuronal polarity, and 3) precise innervation by inhibitory

338   interneurons. The molecular mechanisms regulating these properties all converge on the AIS

339   scaffolding protein AnkG [37,41-43]. However, the distinct proximal mechanisms regulating these

340   AIS properties remain poorly understood, highlighting the need to define the composition of

341   the AIS in much greater detail. BioID-dependent cytoplasmic proximity biotinylation and

342   differential mass spectrometry have partially elucidated AIS proteomes [4,44], but they are clearly

343   deficient in proteins involved in transient interactions, posttranslational modifications, and cell

344   surface proteins mediating extra- and intercellular interactions. Thus, experimental approaches

345   that address these deficiencies are desperately needed.

346   We aimed to use Nfasc-BAR to identify AIS cell surface proteins. The results were highly

347   reproducible at each developmental time point *in vitro*, but showed changing profiles of cell

16

348   surface proteins during development. As expected, our data sets included known AIS cell

349   surface proteins, and consisted almost exclusively of cell surface proteins whose expression

350   levels increased with neuronal maturation. The strategy is highly flexible and can be used with

351   other AIS specific antibodies including those targeting cytoplasmic epitopes after detergent

352   solubilization; the strategy can also be applied to other neuronal compartments including

353   synapses, dendrites, and growth cones so long as highly specific and validated antibodies are

354   used.

355   Since Nfasc is highly enriched at the AIS, we expected AIS-enriched membrane proteins

356   to be over-represented in our data set. However, Nfasc is also found at lower densities in

357   somatodendritic and distal axonal domains, and their total membrane area exceeds that of the

358   AIS. Thus, despite the high density of AIS Nfasc, the total pool of Nfasc in non-AIS membrane is

359   likely much greater. HRP-mediated biotinylation is very efficient and has a range ~25 times

360   greater than BioID or APEX [11]. Thus, the proteins we recovered are more accurately described

361   as an Nfasc surface proximity proteome, with a subset of those proteins also being found at the

362   AIS.

363   Given the promiscuity of Nfasc-BAR, the biggest challenge in our experiments was to

364   determine which proteins to focus on and how to validate their presence or enrichment at the

365   AIS. To this end, we narrowed our analysis using stringent filtering criteria including fold-

366   enrichment, significance of that enrichment, and a minimum number of PSMs recovered. We

367   also estimated the relative proximity to Nfasc based on the ratio of extracellular tyrosine

368   residues to the PSMs recovered. Nfasc-BAR and the filtering criteria used here may

369   underestimate proximity or miss AIS proteins that were not well biotinylated (e.g. ion

Ogawa, Lim et al.

370   channels). Nevertheless, among the proteins recovered and that satisfied the filtering criteria,

371   our use of endogenous gene tagging revealed several that were present or even enriched at the

372   AIS, but that had not been previously described as AIS proteins. In particular, we found that

373   Cntn1 is highly enriched at the AIS. We validated its enrichment there by endogenous gene

374   tagging *in vitro* and *in vivo*, by expression of exogenous epitope-tagged Cntn1 at the AIS *in vitro*

375   and *in vivo*, and by immunostaining of cultured hippocampal neurons using Cntn1 antibodies

376   whose specificity was confirmed using CRISPR-mediated gene disruption. Other candidate AIS

377   proteins (e.g. Tenm4 and Ptprs) will require additional studies to further validate and confirm

378   they are *bona fide* AIS proteins. Additional endogenous gene tagging may reveal more AIS

379   membrane proteins since we only tested a small subset of the Nfasc proximity proteome.

380   The use of numerous methods to confirm that Cntn1 is a *bona fide* AIS protein is

381   important since relying on antibody staining alone can lead to incorrect assignment of a protein

382   being enriched at the AIS [18-20]. Methods allowing CRISPR-mediated endogenous gene tagging

383   are a significant advance to validate protein localization without the confound of off-target

384   antibodies or mislocalization due to over-expression [21-23]. However, the method of tag

385   insertion we used also disrupts coding regions in the last exon of the proteins analyzed, and

386   some proteins that depend on their C-terminal amino acids may be mislocalized. Thus, failure

387   of a protein to localize to the AIS after endogenous gene tagging should not be considered a

388   definitive criterion for exclusion as an AIS protein.

389   Cntn1 is a GPI-anchored cell adhesion molecule that has been studied in the nervous

390   system mainly in the context of its role in axon-glia interactions as an essential component of

391   the paranodal axoglial junction formed between axons and myelinating glia [30]. There, Cntn1

18

Ogawa, Lim et al.

392   participates in cis interactions in the axon with Caspr1 (Contactin ASsociated PRotein 1) and

393   trans interactions with the glial 155 kD form of Nfasc (NF155) [29,45]. Cntn1 can engage in diverse

394   interactions with many cell adhesion and extracellular matrix molecules including Caspr1,

395   members of the L1 family of cell adhesion molecules (Nfasc, NrCAM and L1CAM), Tnr, Tnc, and

396   receptor tyrosine phosphatase β [28,46,47]. Our experiments show that Cntn1's AIS localization

397   requires its first four Ig-like domains and redundant interactions with either Nfasc or NrCAM

398   (Fig. S5a), since only simultaneous deletion of both disrupts Cntn1's AIS localization. In

399   addition, Cntn1 helps assemble the AIS extracellular matrix since its loss affects Tnr

400   recruitment. Future experiments may also reveal roles for Cntn1 in association with other AIS

401   extracellular matrix molecules or membrane proteins including Tnc and Na$^+$ channel β subunits

402   [48]. The importance of Cntn1 in humans is highlighted by the observation that a pathogenic

403   variant of *CNTN1* caused lethal severe fetal akinesia syndrome [49].

404   ChCs and basket cells precisely innervate cortical PyNs and Purkinje neurons,

405   respectively, to regulate AIS excitability. For example, Dudok et al. [38] and Schneider-Mizell et al.

406   [39] showed that a variety of behaviors including pupil dilation, locomotion, and whisking can

407   synchronously activate populations of ChCs to inhibit PyNs through GABAergic synapses.

408   Together, these observations highlight the central role played by ChCs in modulating brain

409   states and behavior. Similarly, pinceau synapses provide strong inhibitory control over Purkinje

410   neuron output, but this is due to ephaptic inhibition rather than chemical inhibition [50]. Despite

411   their importance, the molecular mechanisms responsible for the precise innervation and

412   maintenance of AIS axo-axonic synapses are incompletely understood.

19

413   Loss of AnkG from Purkinje neurons disrupts pinceau synapse formation and has been

414   attributed to mislocalization of AIS NF186; however, loss of ankyrin-binding NrCAM, L1CAM, or

415   CHL1 did not affect pinceau synapse assembly [37]. These observations are consistent with our

416   findings that Cntn1 also regulates pinceau synapse assembly (Fig. S5b), since loss of AnkG

417   affects both NF186 and NrCAM localization [51]. We report here that Cntn1's AIS localization can

418   be independently directed by both of these CAMs (Fig. 6d). This result is consistent with the

419   observation that the specific deletion of NF186 alone in adults does not disrupt pinceau

420   synapse maintenance [52], suggesting that Cntn1 can also partner with other AIS CAMs (e.g.,

421   NrCAM) for synapse maintenance. Since *Cntn1 -/-* mice die by P21, we cannot rule out the

422   possibility that pinceau synapses fail to develop due to widespread developmental defects.

423   Future studies utilizing Purkinje neuron specific deletion of Cntn1 will be required to more

424   precisely define Cntn1's role in pinceau synapse assembly and maintenance.

425   Previously, Tai et al. [41] reported a small RNAi screen of 14 candidate cell adhesion

426   molecules to identify regulators of PyN AIS innervation by ChCs. The candidates screened

427   included Nfasc, NrCAM, and all previously reported AIS CAMs (e.g. Cntn2). Loss of Nfasc,

428   NrCAM, or Cntn2 alone had no effect on ChC/PyN AIS innervation; but the impact of

429   simultaneous loss/depletion of Nfasc and NrCAM remains to be tested. Importantly, among the

430   candidates screened, only loss of L1CAM significantly reduced PyN AIS synaptic innervation by

431   ChCs, despite the fact that L1CAM is found not only at the AIS, but along the entire axon [25].

432   This suggests that L1CAM may cooperate in cis with other membrane or adhesion molecules

433   like Cntn1 for precise innervation of the AIS by ChCs (Fig. S5c). In addition to L1CAM, Hayano et

434   al. [53] reported the cell adhesion molecule Igsf11 functions both pre- and post-synaptically in

Ogawa, Lim et al.

435   layer 2/3 of cortex to regulate assembly of PyN/ChC axo-axonic synapses. However, we did not

436   find Igsf11 in our Nfasc-BAR results at any time point; although this may reflect Igsf11 having

437   relatively few extracellular tyrosines. Alternatively, there may be differences between neurons

438   *in vitro* and *in vivo*, or even between types of neurons.

439   One limitation of this study is that the proximity biotinylation experiments were

440   performed on cultured neurons. AIS cell surface proteins whose localization depends on the

441   native brain environment may not be represented. For example, AIS GABAergic synapses may

442   form *in vitro*, but they are rare, making it difficult to identify presynaptic receptor(s) for Cntn1

443   and L1CAM using Nfasc-BAR. Future experiments using extracellular split TurboID [54], where

444   PyNs and ChCs each express one half of TurboID may help to identify the pre-synaptic receptor

445   found on ChCs. Alternatively, developing *in situ* Nfasc-BAR for use with brain tissue may reveal

446   additional AIS cell surface proteins and their receptors.

447   In summary, we used extracellular proximity biotinylation to identify Cntn1 as a new AIS

448   adhesion molecule. Cntn1 is restricted to the AIS through its binding to AnkG-localized Nfasc or

449   NrCAM (Fig. S5a). In Purkinje neurons, Cntn1 is required for AIS innervation by basket cells (Fig.

450   S5b). In PyNs, Cntn1 functions together with L1CAM to regulate the AIS-specific targeting and

451   developmental assembly of PyN/ChC axo-axonic synapses (Fig. S5c). Thus, our results suggest a

452   model where axo-axonic innervation of diverse neuron types converges on AIS-enriched Cntn1.

453

454

METHODS

Animals

Timed pregnant Sprague-Dawley rats were obtained from Charles River Laboratories. Rats were euthanized for embryo collection at E18. Brains were collected from *Cntn1 -/-* and *+/-* mice at P17 (catalog #Jax:034216, RRID:IMSR_JAX:034216). The *Cntn1* mice were maintained at the Weizmann Institute of Science, Rehovot, Israel. P0 ICR mice were used for intraventricular injection of AAV for overexpression of Cntn1-Myc. Transgenic Cas9 mice (catalog #Jax: 027650, RRID: IMSR_JAX:027650) were used for intraventricular injection of AAV to perform tagging of endogenous Cntn1. Nkx2-1$^{tm1.1(Cre/ERT2)Zjh}$/J and B6;129S6-Gt(Rosa)26Sor$^{tm9(CAG-tdTomato)Hze}$/J were a gift from Dr. Z.J. Huang [55]. Swiss Webster mice were purchased from Charles River (Cat# CRL:24; RRID: IMSR_CRL:24). All experiments were performed in compliance with the National Institutes of Health Guide for the Care and Use of Laboratory Animals and were approved by the Baylor College of Medicine, the Cold Spring Harbor, and the Weizmann Institute of Sciences Institutional Animal Care and Use Committees.

Cell Culture

Primary cultures of hippocampal neurons were obtained from E18 Sprague-Dawley rat embryos. Hippocampi were dissected and dissociated. For imaging, neurons were plated onto Poly-D-Lysine (Sigma) and laminin-coated glass coverslips (Life Technologies) at a density of ~1.25 X 10^4 cells/cm^2. For mass spectrometry, neurons were plated onto Poly-D-Lysine and laminin-coated 10 cm dishes at a density of ~2.5 X 10^4 cells/cm^2. Hippocampal neurons were maintained in Neurobasal medium (Life Technologies) containing 1% Glutamax (Life

Ogawa, Lim et al.

477   Technologies), 1% penicillin and streptomycin (Life Technologies), and 2% B27 supplement (Life

478   Technologies) in an incubator at 37°C with 5% CO_2.

479

480   ***Biotinylation by Antibody Recognition***

481   Cultured rat primary neurons (~2 × 10^6 primary hippocampal neurons for each

482   condition) were biotinylated at each of 5 different timepoints. Cells were live labeled by

483   incubating with primary antibodies diluted in culture media for 1 hr at 37°C, then washed with

484   neurobasal media and incubated in culture media alone for 1 hr at 37°C. Cells were incubated

485   with horseradish peroxidase (HRP)-labeled secondary antibodies diluted in culture media for 30

486   min at 37°C, then washed with PBS. Biotin tyramide (Perkin Elmer Cat# NEL749A001KT) was

487   diluted 1:500 in a dilution buffer containing H_2O_2, and applied to cells for 5 min at 4°C. Cells

488   were washed with PBS and lysed in RIPA buffer (50 mM Tris-HCl, 150 mM NaCl, 0.5% sodium

489   deoxycholate, 0.1% SDS, and 1% NP-40). Biotinylated proteins were isolated using streptavidin

490   magnetic sepharose beads (GE Healthcare Cat# 28-9857-38) overnight at 4°C and then washed

491   seven times in RIPA buffer. Control cells were labeled and processed using the same steps

492   except for the omission of primary antibodies.

493

494   ***Mass Spectrometry.***

495   Sample-incubated streptavidin magnetic sepharose beads were resuspended in 5 mM

496   DTT in 100 mM NH_4HCO_3 and incubated for 30 min at room temperature. After this,

497   iodoacetamide was added to a final concentration of 7.5 mM and samples incubated for 30

498   additional minutes. In all, 0.5 µg of sequencing grade trypsin (Promega) was added to each

23

499　sample and incubated at 37°C overnight. Supernatants of the beads were recovered, and beads

500　digested again using 0.5 μg trypsin in 100 mM NH_4HCO_3 for 2 h. Peptides from both consecutive

501　digestions were recovered by solid phase extraction using C18 ZipTips (Millipore, Cat#

502　ZTC18S096), and resuspended in 0.1% formic acid for analysis by liquid chromatography-mass

503　spectrometry (LC-MS/MS). Peptides resulting from trypsinization were analyzed on a QExactive

504　Plus (Thermo Scientific), connected to a NanoAcquity™ Ultra Performance UPLC system

505　(Waters). A 15-cm EasySpray C18 column (Thermo Scientific) was used to resolve peptides (90-

506　min gradient with 0.1% formic acid in water as mobile phase A and 0.1% formic acid in

507　acetonitrile as mobile phase B). MS was operated in data-dependent mode to automatically

508　switch between MS and MS/MS. The top ten precursor ions with a charge state of 2^+ or higher

509　were fragmented by high-energy collisional dissociation. Peak lists were generated using PAVA

510　software [56]. All generated peak lists were searched against the rat subset of the UniProt

511　database (UniprotKB 2017.11.01) using Protein Prospector [57]. The database search was

512　performed with the following parameters: a mass tolerance of 20 ppm for pre- cursor masses;

513　30 ppm for MS/MS, cysteine carbamidomethylation as a fixed modification and acetylation of

514　the N terminus of the protein, pyroglutamate formation from N-terminal glutamine, and

515　oxidation of methionine as variable modifications. All spectra identified as matches to peptides

516　of a given protein were reported, and the number of spectra (Peptide Spectral Matches, PSMs)

517　used for label free quantitation of protein abundance in the samples.

518

519　***Antibodies***

Ogawa, Lim et al.

520   The following antibodies were used for *in vitro* biotinylation (dilutions for each antibody

521   are indicated in parentheses): chicken polyclonal antibody anti-neurofascin (1:1000; R&D

522   Systems Cat# AF3235, RRID:AB_10890736), rabbit polyclonal anti-NrCAM (1:1000; Abcam Cat#

523   ab24344, RRID:AB_448024), anti-chicken HRP-labeled secondary antibody (1:2000; Aves Labs

524   Cat# H-1004, RRID:AB_2313517), anti-rabbit HRP-secondary antibody (1:2000; Jackson

525   ImmunoResearch Labs Cat# 111-035-003, RRID:AB_2313567).

526   The following antibodies were used for immunofluorescence studies (dilutions for each

527   antibody are indicated in parentheses): chicken polyclonal anti-neurofascin (1:500; R&D

528   Systems Cat# AF3235, RRID:AB_10890736), chicken polyclonal anti-MAP2 (1:1000; EnCor

529   Biotechnology Cat# CPCA-MAP2, RRID:AB_2138173), mouse monoclonal anti-Ankyrin-G (1:500;

530   NeuroMab N106/36, RRID:AB_10673030), mouse monoclonal anti-Tenascin-R (1:250; R&D

531   Systems Cat# MAB1624, RRID:AB_2207001), rabbit polyclonal anti-NrCAM (1:250; Abcam Cat#

532   ab24344, RRID:AB_448024), rabbit polyclonal anti-β4 spectrin (1:500, Rasband lab,

533   RRID:AB_2315634), rabbit polyclonal anti-Kv1.2 (1:250, James Trimmer, University of California,

534   Davis, RRID:AB_2756300), mouse monoclonal anti-PSD-95 (1:250; Antibodies Incorporated Cat#

535   75-028, RRID:AB_2292909), mouse monoclonal anti-Tuj1 (1:700; BioLegend Cat# 801202,

536   RRID:AB_10063408), goat polyclonal anti-Cntn1 (1:500; R&D Systems Cat# AF904,

537   RRID:AB_2292070), mouse monoclonal anti-Myc (1:2000; MBL International Corporation Cat#

538   M192, PRID: AB_11160947), rat monoclonal anti-HA (1:500; Millipore Sigma Cat# 11867423001,

539   RRID: AB_390918), mouse monoclonal anti-V5 (1:500; Invitrogen Cat# R960CUS, RRID:

540   AB_159298). Anti-RFP (guinea pig pAb, 1:1000, Synaptic systems 390 005), anti-gephyrin

25

Ogawa, Lim et al.

541   (mouse mAb IgG1, 1:500, Synaptic Systems 147 011), and anti-VGAT (guinea pig pAb, 1:500,

542   Synaptic Systems 131 004).

543   The following secondary antibodies were used: Alexa Fluor 555 goat anti-rat (1:1000,

544   Thermo Fisher Scientific A-11006), Alexa Fluor Plus 555 goat anti-rabbit (1:1000, Thermo Fisher

545   Scientific A32732), Alexa Fluor 647 goat anti-rabbit (1:1000, Thermo Fisher Scientific A-21244),

546   Alexa Fluor 555 goat anti-guinea pig (1:1000, Thermo Fisher Scientific A-21435), Alexa Fluor 647

547   goat anti-guinea pig (1:1000, Thermo Fisher Scientific A-21450), Alexa Fluor 647 goat anti-

548   mouse IgG1 (1:1000, Thermo Fisher Scientific A-21240), Alexa Fluor 488 goat anti-mouse IgG2a

549   (1:1000, Thermo Fisher Scientific A-21131), Aminomethylcoumarin (AMCA) anti-chicken IgY

550   (1:1000 Jackson Immunoresearch labs 103-155-155), Alexa Fluor 488 anti-chicken IgY, (1:1000

551   Jackson Immunoresearch labs 103-545-155), Alexa Fluor 488 anti-mouse IgG (1:1000 Thermo

552   Fisher Scientific A11029), Alexa Fluor 594 anti-rabbit (1:1000 Thermo Fisher Scientific A11034),

553   Alexa Fluor 594 anti-mouse IgG (1:1000 Thermo Fisher Scientific A32742). Streptavidin Alexa

554   Fluor 594 conjugates were purchased from Thermo Fisher Scientific (1:5000; S11227). Hoechst

555   fluorescent reagent (1:100,000; Thermo Fisher Scientific Cat# H3569, RRID:AB_2651133) was

556   used to label nuclei.

557

558   ***In Utero* Electroporation and Tamoxifen Induction**

559   To manipulate Cntn1 expression in pyramidal neurons (PyNs) and sparsely label

560   chandelier cells (ChCs) in the same neocortical layer, ventricular zone-directed *in utero*

561   electroporation targeting neocortical PyN progenitors was performed in *Nkx2.1-CreER;Rosa26-*

562   *loxpSTOPloxp-tdTomato (Ai9)* embryos. Specifically, Swiss Webster females were bred with

Ogawa, Lim et al.

563 *Nkx2.1-CreER⁺ᐟ⁻;Ai9⁺ᐟ⁺* males. Pregnant females at 15.5 days of gestation were anesthetized, the

564 uterine horns were exposed, and approximately 1 µl of plasmid solution (0.75 µg/µl pCAG-

565 1BPNLS-Cas9-1BPNLS + 1.5 µg/µl pAAV-3x-sgRNA-smFP (with control or target specific sgRNAs;

566 see STAR Methods) was injected manually into the lateral ventricle of the embryos using a

567 beveled glass micropipette (Drummond Scientific). After injection, five square 50 ms pulses of 45

568 V with 950 ms intervals were delivered across the uterus with two 5 mm electrode paddles (BTX,

569 45-0489) positioned on either side of the head (BTX, ECM830). After electroporation, the uterine

570 horns were placed back in the abdominal cavity of the pregnant dam and the wound was

571 surgically sutured. Tamoxifen (3 mg/30 g of body weight) was administered to the pregnant dam

572 by oral gavage at 18.5 days of gestation to induce CreER activity and excision of the STOP cassette,

573 resulting in tdTomato red fluorescent protein expression in a sparse population of nascent

574 neocortical ChCs in their offspring. Pups were euthanized at postnatal day 17.

575

576 ***Immunofluorescence labeling***

577 Cultured rat primary hippocampal neurons were fixed in 4% paraformaldehyde (PFA, pH

578 7.2) for 15 minutes at 4°C. Acutely dissected brains were drop fixed in 4% paraformaldehyde

579 (PFA, pH 7.2) for 60 minutes at 4°C. Brains were then equilibrated overnight in 20% and 30%

580 sucrose in 0.1 M PB overnight at 4°C. Brains were then sectioned at 12-25 µm and mounted on

581 coverslips. Fixed neurons and brain sections were permeabilized and blocked with 10% normal

582 goat serum in 0.1 M PM with 0.3% Triton X-100 (PBTGS) for one hour. Cells and sections were

583 then incubated in primary antibodies diluted in PBTGS overnight at room temperature or 4°C.

584 Tissues and cells were then washed three times using PBTGS for 5 min. each. Fluorescent

27

Ogawa, Lim et al.

585 secondary antibodies were then diluted in PBTGS and added to cells and tissues for one hour.

586 Coverslips were then washed once using PBTGS, 0.1 M PB, and finally 0.05 M PB for 5 min.

587 each. Coverslips were then mounted using Vectashield plus (vector labs) anti-fade mounting

588 media.

589 For immunostaining of electroporated neonatal brains, P17 mice were deeply

590 anesthetized with isoflurane and perfused transcardially with PBS and 4% paraformaldehyde

591 (PFA) in 0.1 M phosphate buffer. Brains were post-fixed in 4% PFA in 0.1 M phosphate buffer

592 overnight at 4°C and then cryoprotected with 30% sucrose in PBS. 50 μm thick coronal sections

593 were subsequently generated using a Vibratome (Leica VT1000S). For gephyrin and VGAT

594 immunostaining, brain slices were subjected to mild antigen retrieval with 10 mM citrate buffer

595 for 30 minutes at 60°C. Subsequently, brain slices were blocked and permeabilized with 10%

596 normal goat serum (NGS) and 0.3% Triton X-100 in PBS at RT for 30 minutes and then incubated

597 with primary antibodies diluted in 2% NGS and 0.3% Triton X-100 in PBS overnight at 4°C.

598 Fluorescent secondary antibodies diluted in 2% NGS and 0.3% Triton X-100 in PBS were applied

599 for 2 h at RT the following day. Sections were then washed three times with PBS for 20 min per

600 wash and mounted with Fluoromount-G (Southern Biotech).

601

602 **Plasmid construction**

603 The sgRNAs and the homology-independent donor templates were generated following

604 strategies similar to those described previously [19,22,23,58]. Briefly, the U6 promoter and scaffold

605 sequences were PCR amplified from pMJ117 and pMJ179 (gifts from Jonathan Weissman,

28

Ogawa, Lim et al.

606   Addgene plasmid #85997 and #85996). The smFP-V5 (a gift from Loren Looger, Addgene

607   plasmid #59758) was used as a knock-in donor.

608   The knockout constructs expressing three independent sgRNAs and a smFP-HA marker

609   (pAAV-3x-gRNA-smFP) were generated as follows: the U6 promoter and scaffold sequences

610   were PCR amplified from pMJ114, pMJ117, and pMJ179 (gifts from Jonathan Weissman,

611   Addgene plasmid # 85995, #85997, and #85996). Human Synapsin1 promoter and smFP-HA

612   were PCR amplified from pAAV-hSyn-EGFP (a gift from Bryan Roth, Addgene Plasmid #50465)

613   and pCAG_smFP-HA (a gift from Loren Looger, Addgene plasmid #59759), respectively. The

614   plasmid PX552 (a gift from Feng Zhang, Addgene plasmid #60958) was digested with a *NotI*

615   restriction enzyme (NEB) and used as a plasmid backbone. DNA fragments were ligated

616   together using an In-Fusion Snap Assembly Master Mix (Takara).   The sgRNA sequences for

617   knock-in and knockout are listed in the supplemental materials table. The AAV-SpCas9 plasmid

618   (a gift from Feng Zhang, Addgene plasmid #60957) was modified by removing the HA tag.

619   Cntn1 constructs were generated in both pcDNA3 and AAV backbones. pcDNA3 was

620   digested with *EcoRI* restriction enzyme (NEB) and pAAV-hSyn-EGFP (a gift from Bryan Roth,

621   Addgene Plasmid #50465) was digested with *BamHI* and *XhoI* restriction enzymes (NEB) and

622   used as plasmid backbones. Full-length and truncated Cntn1 was PCR amplified from rat

623   contactin-myc [34] and ligated together using an In-Fusion Snap Assembly Master Mix (Takara).

624   All DNA constructs were verified by sequencing (Genewiz and plasmidsaurus).

625

626   ***Adeno-associated virus (AAV) production***

29

627 Small scale AAV cell-lysates were produced using the AAVpro Purification Kit (All Serotypes)

628 (Takara) with slight modifications. Briefly, HEK293T cells were triple-transfected with AAV

629 plasmid, helper plasmid (Agilent Technologies, Cat # 240071), and serotype PHP.S or PHP.eB

630 plasmids (a gift from Viviana Gradinaru, Addgene plasmids #103002 and #103005) with PEI Max

631 (Polysciences, Cat # 24765). The medium was changed the next day of transfection and cells

632 were incubated for 3 days after transfection. HEK cells were then collected and lysed with the

633 AAV Extraction Solution A plus. The extracted solution was centrifuged at 10,000 x g for 10 min

634 to remove debris and mixed with Extraction Solution B. This small scale AAV solution was stored

635 at 4°C and used for neuronal transduction into cultured neurons. AAV vectors for *in vivo*

636 transduction were produced by the Baylor College of Medicine Neuroconnectivity Core or in

637 our lab following the strategies described previously [59].

638

639 ***Viral transduction of neurons***

640 For viral transduction of cultured neurons, 10 µl of AAV-Cas9 and 10 µl of AAV-sgRNA and

641 donor, or AAV-3x-sgRNA-smFP, were added into a well of a 12-well plate at 0-1 DIV. The

642 medium was replaced 2 days after infection. For viral transduction of neurons *in vivo*, AAV

643 vectors were injected into the lateral ventricles of neonatal mice as described previously [60].

644 Briefly, P0 to P2 pups were anesthetized on ice and 1-2 µl of AAV vectors were bilaterally

645 injected. The pups were placed in a heated cage until the animals recovered and then returned

646 to their mother. For transduction of neurons in adult, viruses were injected retro-orbitally in 13

647 week-old C57Bl/6J mice. Tissues were collected 4 weeks after infection.

648

649 ***Confocal Image Acquisition and Analysis of ChC/PyN AIS Innervation and GABAergic Synapse***

650 ***Density at PyN AISs***

651 For analysis of ChC/PyN AIS percent innervation, images of coronal brain slices (50 μm thick) were

652 acquired using an LSM 800 confocal laser-scanning microscope (Zeiss) with a 63x oil-immersion

653 objective and sequential acquisition settings applied at a resolution of 1024x1024 pixels. 200 μm

654 x 200 μm images of single RFP+ ChCs and neighboring GFP+ electroporated PyNs in layer II of the

655 somatosensory cortex were collected using a z series of 30-36 images with a depth interval of 1

656 μm. ChC/PyN AIS percent innervation was calculated by dividing the number of GFP+ PyNs

657 innervated at their AIS by a single RFP+ ChC by the total number of GFP+ PyNs in the entire 200

658 μm x 200 μm image z stack. Representative maximum projection images were generated from

659 10 z-series images with a depth interval of 1 μm. To quantify the average density of gephyrin or

660 VGAT puncta per μm on the AIS of PyNs, 90 μm x 90 μm images were acquired at a resolution of

661 1280x1280 pixels using a z-series of 40-60 images with a depth interval of 0.37 μm. The number

662 of gephyrin or VGAT puncta overlapping with AnkG+ or β4-spectrin+ PyN AISs in individual z-

663 plane images was manually counted and AIS lengths were measured using Zeiss Zen (Blue Edition)

664 imaging software. Gephyrin or VGAT puncta density at the AIS was then calculated by dividing

665 the number of PyN AIS gephyrin or VGAT puncta by the length of the AIS. Representative

666 maximum projection images of PyN AIS GABAergic synapses visualized via gephyrin or VGAT

667 immunostaining were generated using a z-series of 10 images with a depth interval of 0.37 μm.

668

669 ***Image Acquisition***

Ogawa, Lim et al.

670   Images of immunofluorescence were captured using an Axio-imager Z2 microscope fitted with

671   an apotome attachment for structured illumination (Carl Zeiss MicroImaging) and a Nikon

672   Eclipse Ni2. 20X (0.8 NA), 40X (0.95 NA), and 63X (1.4 NA) objectives were used. Images were

673   taken using Zen 3.2 (Zeiss) or NIS-Elements (Nikon). For measurements of AIS streptavidin

674   fluorescence intensity, 20 neurons per timepoint per replicate were imaged and line scans were

675   drawn using Zen 3.2 software. Images were exported to Fiji, Adobe Photoshop, and Adobe

676   illustrator for figure presentation. Some figures were generated using Biorender.

677

678   ***Statistical Analysis and Quantification***

679   Unpaired, two-tailed Student's *t*-test was used for all statistical analyses unless otherwise

680   indicated. Data were analyzed using Microsoft Excel and GraphPad Prism. All error bars are

681   ±SEM unless otherwise indicated. PSMs were normalized using the formula $PSM_{Norm} = PSM_{DIVX}$ *

682    $Csum_{Max}$ / $Csum_{DIVX}$. PSM_{DIVX} is the raw PSM count for a candidate protein for a particular

683   replicate at the specified timepoint; $Csum_{Max}$ is the maximum sum of seven endogenously

684   biotinylated carboxylases Acaca, Acacb, Pc, Pcca, Pccb, Mccc1, Mccc2 for an individual replicate

685   across all 15 replicates; $Csum_{DIVX}$ is the sum of seven endogenously biotinylated carboxylases

686   Acaca, Acacb, Pc, Pcca, Pccb, Mccc1, Mccc2 for an individual replicate at the specified timepoint

687   DIVX. Heatmaps were generated using GraphPad Prism. Candidates were rank-ordered by the

688   slope of the linear regression of their log_2 fold enrichment over time. The number of

689   extracellular tyrosines for proteins whose log_2 fold change was > 2 and that had at least ten

690   PSMs were counted using a script that extracted protein topology from the Uniprot database

32

Ogawa, Lim et al.

691   (www.uniprot.org). The tyrosine-PSM proximity plot was generated using Python

692   (www.python.org). Colors were added in Adobe Illustrator.

693

694   ***Extended materials***

695   A detailed list of all materials including all gRNA sequences, antibodies, plasmids,

696   sources, etc. is provided in the supplemental extended materials file.

697 **ACKNOWLEDGEMENTS**

701

702 **AUTHOR CONTRIBUTIONS**

703 Conceptualization methodology, validation, investigation, visualization, and writing— reviewing

704 and editing: Y.O. and B.C.L.; Investigation, analysis, and writing – reviewing and editing: S.G.;

705 Investigation and analysis: J.M.R., Y.E-E., and F.B.; Investigation, data curation: J.O-P.;

706 Resources, supervision, funding acquisition, and writing – reviewing and editing: A.L.B., E.P.,

707 and L.V.A.; Conceptualization, methodology, data curation, writing— original draft and editing,

708 project administration, and funding acquisition: M.N.R.

709

710 **COMPETING INTERESTS**

711 The authors declare no competing interests.

712

713 **DATA AVAILABILITY STATEMENT**

714 All mass spectrometry data sets from experiments included here are deposited at PRIDE

715 (Proteomics Identifications Database).

716

Ogawa, Lim et al.

717 **FIGURES**
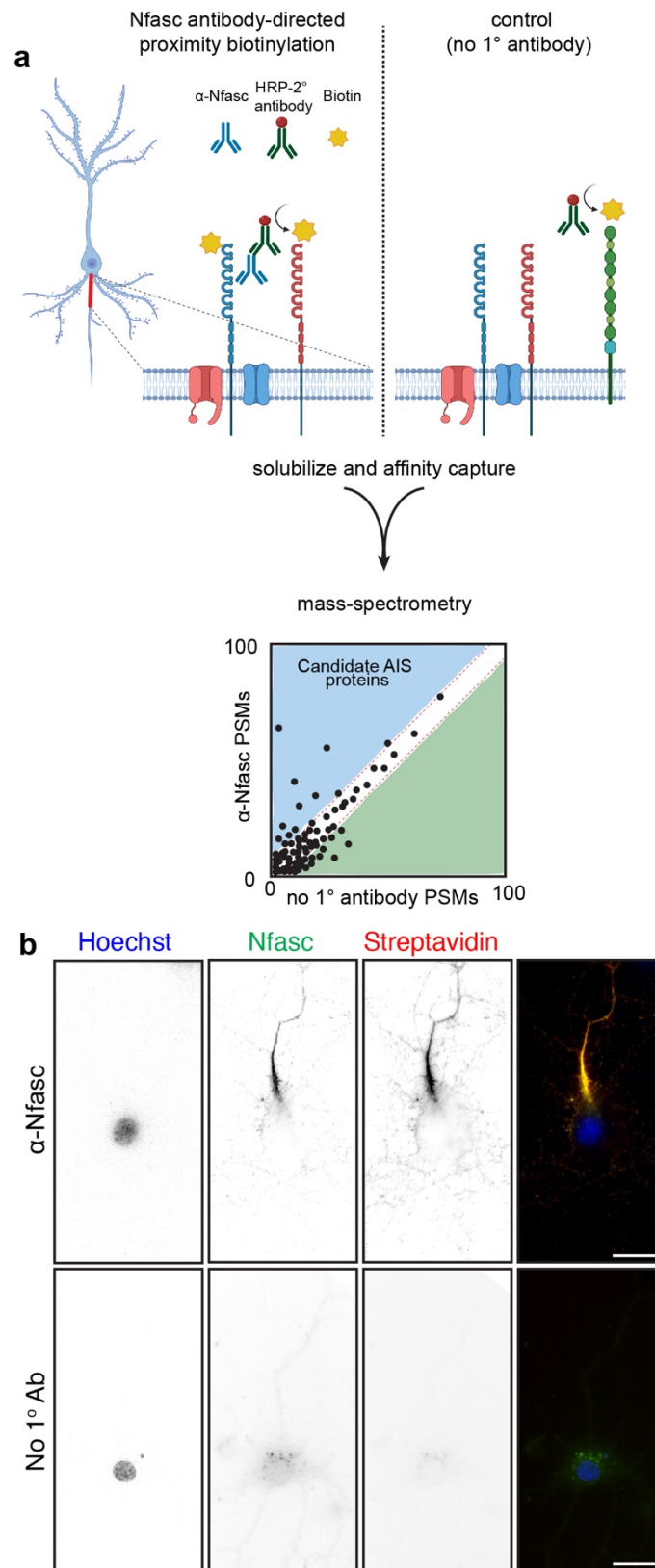
718

Ogawa, Lim et al.

719 **Figure 1. Proximity-dependent biotinylation using Nfasc antibodies. a,** Illustration of the

720 antibody-directed proximity biotinylation strategy. Anti-Nfasc antibodies bind to Nfasc, while

721 HRP-conjugated secondary antibodies bind to the Nfasc antibodies. Addition of biotin phenol

722 (biotin tyramide) in an H_2O_2 containing diluent results HRP-mediated conversion of the biotin

723 phenol to an active radical biotin phenoxyl that covalently adds the tyramide biotin to

724 extracellular tyrosine residues. Omission of the primary anti-Nfasc serves as a control. After

725 stringent solubilization and affinity capture by streptavidin-conjugated magnetic beads.

726 Biotinylated proteins are then identified by mass spectrometry. **b,** Fluorescence imaging of

727 DIV14 rat hippocampal neurons labeled by Nfasc-BAR or a control condition (no primary Ab).

728 Nfasc fluorescence (green) enrichment defines the AIS. Biotinylated proteins were detected

729 using Alexa594-conjugated streptavidin. Scale bars, 20 μm.

Ogawa, Lim et al.

Ogawa, Lim et al.

731
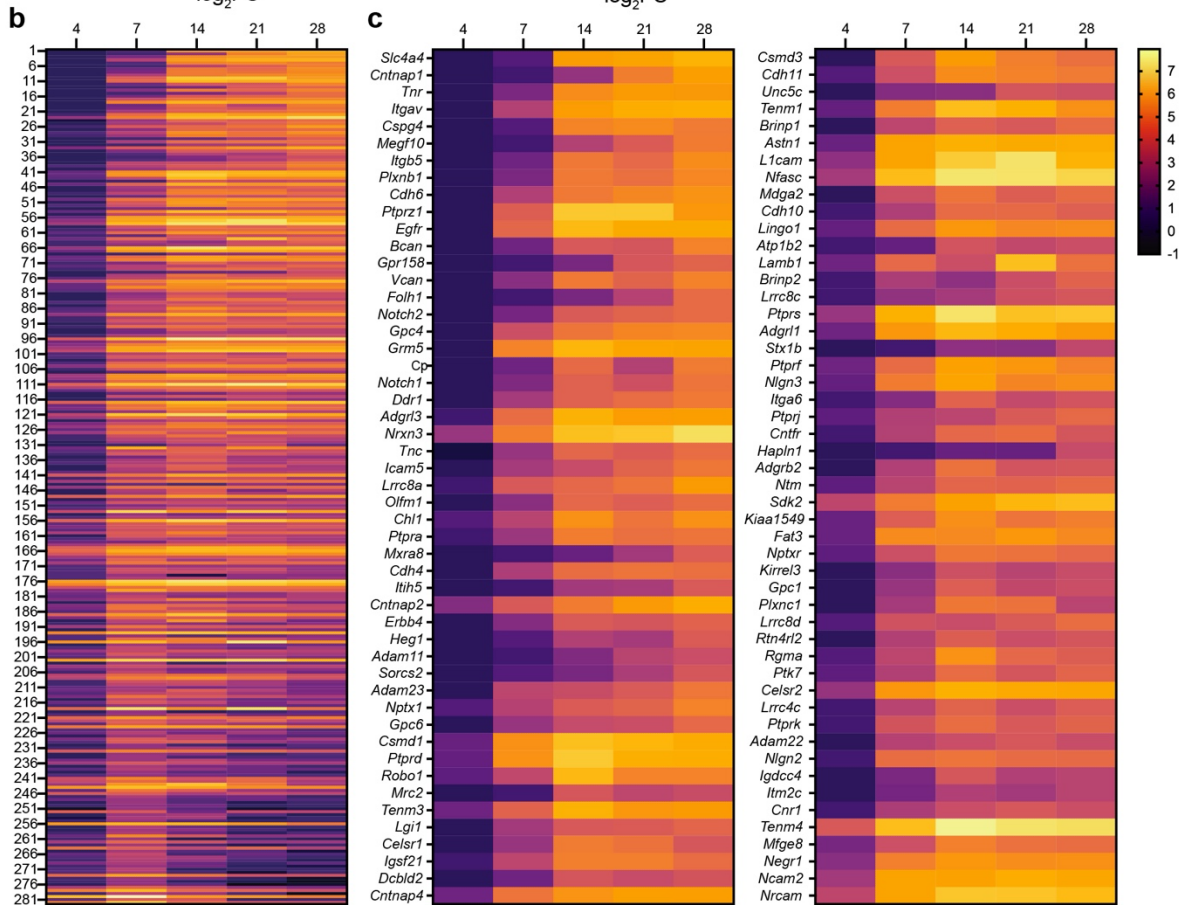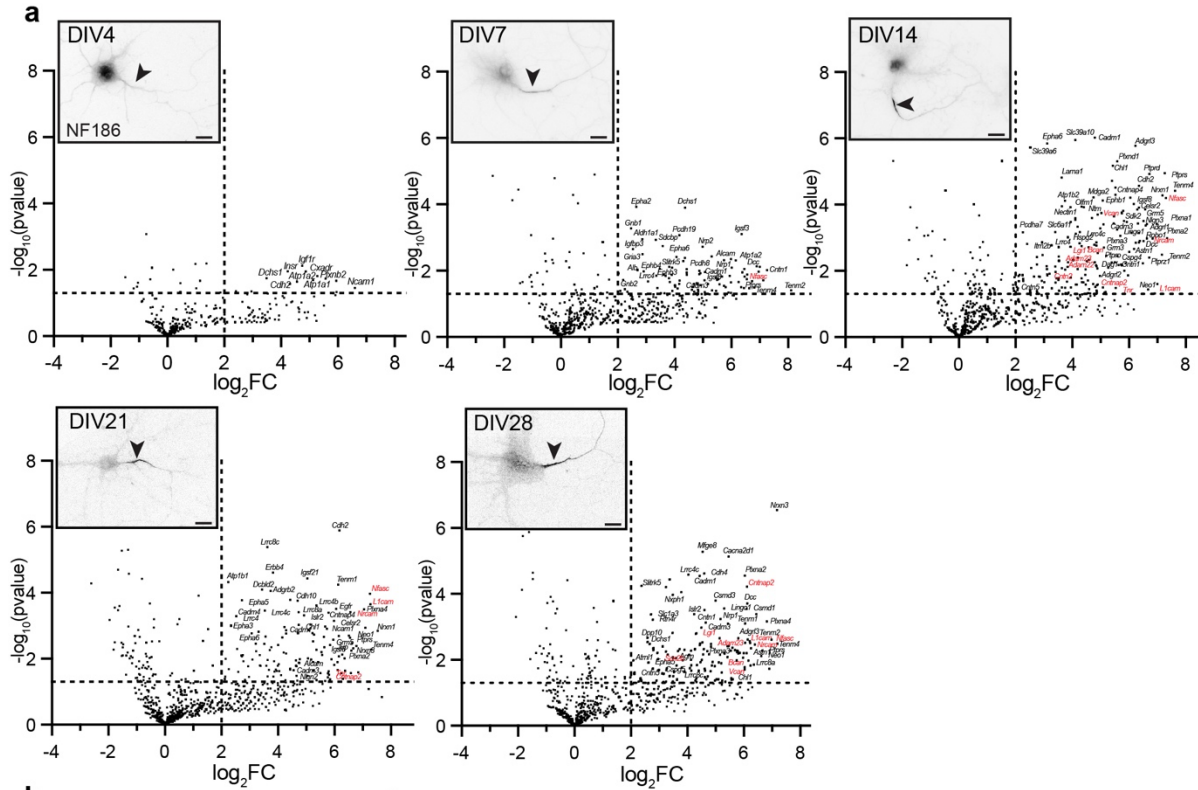
732 **Figure 2. NF186 proximity proteomes across neuronal development. a,** Volcano plots showing

733 the $\log_2$-fold changes of proteins versus the statistical significance -$\log_{10}$(pvalue) identified using

734 Nfasc-directed proximity biotinylation (N=3). $p<0.05$ was used as a cutoff for significance

735 (horizontal dashed line). Some identified proteins are indicated (corresponding gene names

736 listed), with those previously reported as AIS cell surface proteins in red, respectively. Inset

737 images show immunofluorescence labeling of NF186 at different timepoints of hippocampal

738 neuron development *in vitro*. Lower panels: magnified images show the Nfasc-labeled AIS at

739 each time point. Scale bars, 20 μm. **b,** Heatmaps showing $\log_2$-fold changes at each timepoint

740 for all 285 proteins that satisfied two filtering criteria [(1) normalized PSMs > 10; (2) $\log_2$FC

741 (Nfasc/Ctrl) > 2] for at least one of five timepoints, rank-ordered by the slope of the linear

742 regression of their $\log_2$ fold enrichment over time. **c,** Expanded heat map showing gene names

743 for the proteins (1-50 and 51-100) with the largest rate of increase in PSM count (B). Data

744 shown are from N = 3 replicates for each timepoint (see Figure S2).

745

746
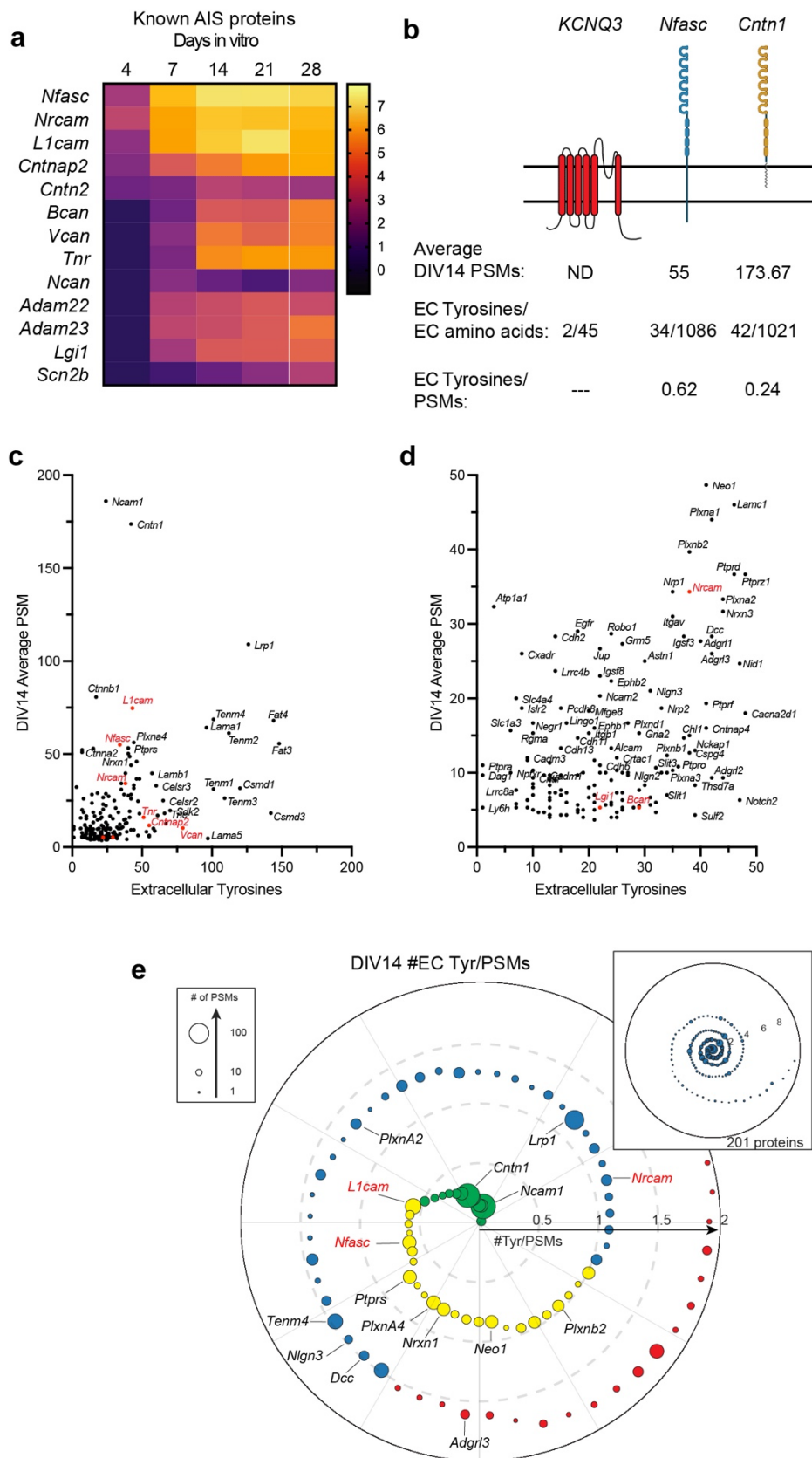
Ogawa, Lim et al.

Ogawa, Lim et al.

748   **Figure 3. Nfasc-BAR identifies known AIS membrane and membrane-associated proteins. a,**

749   Known AIS membrane and membrane associated proteins and their log$_2$FC (Nfasc/Ctrl). **b,**

750   Illustration of membrane topology, average PSMs (at DIV14), and the number of extracellular

751   tyrosine residues for three different AIS and membrane proteins. Figure generated using

752   Biorender. **c, d,** Scatter plot of the number of peptide spectral matches (PSMs) for each

753   biotinylated protein identified by mass spectrometry as compared to the number of tyrosine

754   residues present in each protein's extracellular domain, shown at different scales. Proteins in

755   red were previously reported at the AIS. **e,** Proximity plot showing biotinylated proteins (at

756   DIV14) ordered by extracellular (EC) tyrosine/PSM ratio. The plot is an estimate of abundance

757   and proximity to the HRP secondary antibody bound to the Nfasc primary antibody. Each

758   protein is represented by a circle with size proportional to the number of PSMs identified for

759   that protein. Proteins analzyed in subsequent experiments are indicated by their gene names.

760   EC Tyrosine/PSM ratio: 0-0.5 green, 0.5-1.0 yellow, 1.0-1.5 blue, 1.5-2.0 red.

761
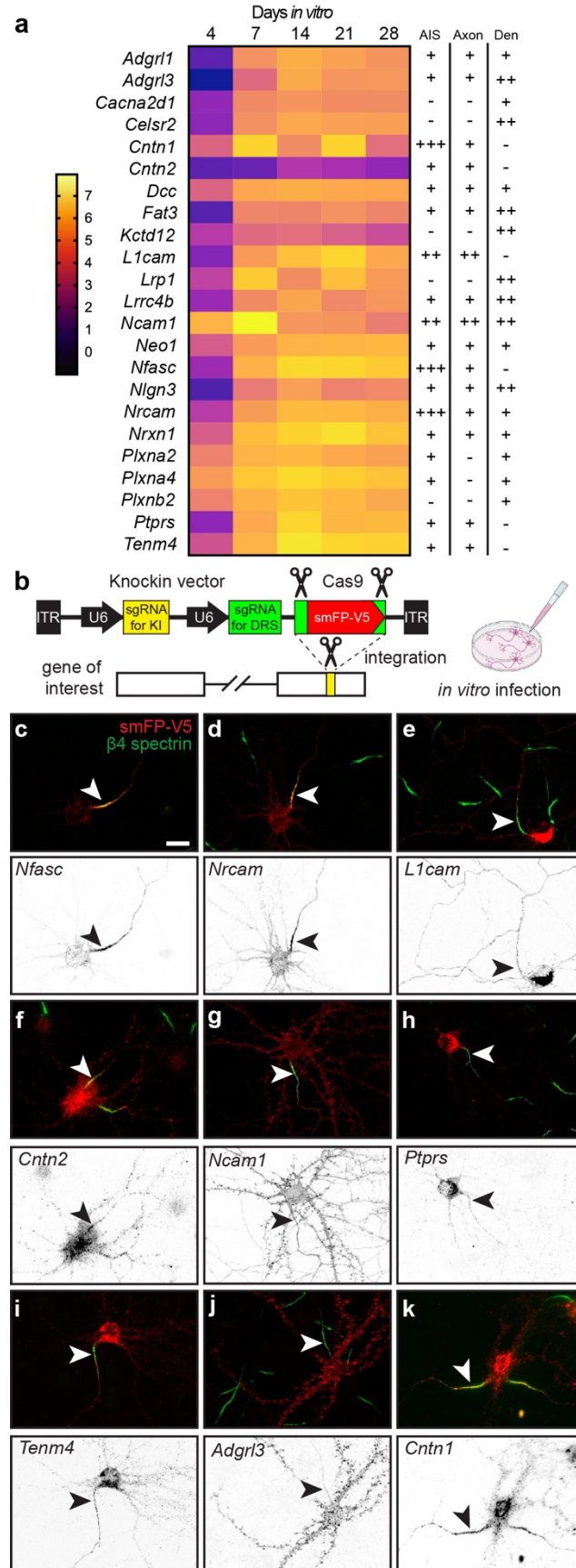
Ogawa, Lim et al.

763 **Figure 4. Tagging of endogenous membrane proteins. a,** Proteins whose distribution was

764 tested using endogenous protein tagging. The heatmap shows the increase in expression level

765 is shown as a function of days *in vitro* (see also Figure 2c). The presence of the tagged protein

766 in AIS, axon, and dendrite is indicated. **b,** Schematic of the knock-in vector for *in vitro* CRISPR-

767 mediated endogenous gene tagging. DRS, donor recognition sites. **c-k,** Examples of smFP-V5

768 tagged proteins (red) enriched at the AIS (c, d, f, k), the axon (e, g), dendrites (j), or in multiple

769 domains (e, g, h, i). AIS are labeled for β4 spectrin (green) and are indicated by an arrowhead.

770 Scale bar, 20 μm.

771

Ogawa, Lim et al.
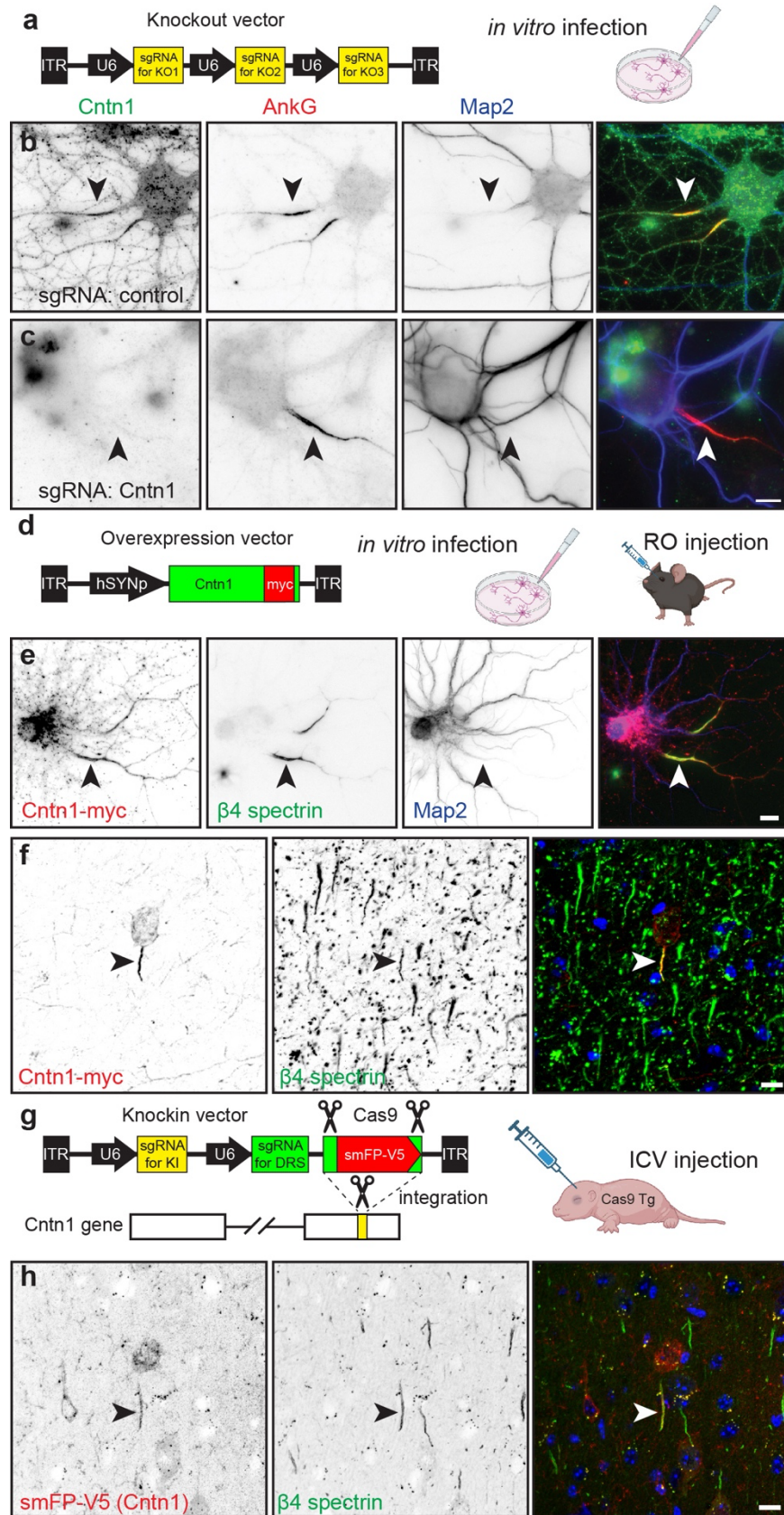
772

Ogawa, Lim et al.

773

774   **Figure 5. Cntn1 is a *bona fide* AIS protein. a,** Schematic of the knockout vector including 3

775   sgRNAs targeting the gene of interesting. The AAV generated using this vector were used for *in*

776   *vitro* transduction of neurons. **b, c,** Immunostaining for Cntn1 (green), AnkG (red) and Map2

777   (blue) after transduction with AAV to Cas9 and control (b) or Cntn1 (c) sgRNAs. Neurons

778   transduced with the Cntn1 sgRNAs lacked AIS Cntn1, but retained robust AnkG at the AIS. AIS

779   are indicated by the arrowheads. Scale bar, 10 μm. **d,** Schematic of the Cntn1-myc

780   overexpression vector used for *in vitro* and *in vivo* infection of neurons. **e,** Transduction of

781   cultured hippocampal neurons using AAV to express Myc-tagged Cntn1. Cntn1-myc (red) is

782   enriched at the AIS (arrowhead) where it colocalizes with β4 spectrin (green). The

783   somatodendritic domain is identified using antibodies against Map2 (blue). Scale bar, 10 μm. **f,**

784   *In vivo* transduction of cortical neurons using AAV to express Myc-tagged Cntn1. Cntn1-myc

785   (red) is enriched at the AIS (arrowhead) where it colocalizes with β4 spectrin (green). Nuclei are

786   labeled using Hoechst dye (blue). Scale bar, 10 μm. **g,** Schematic of the knock-in vector for *in*

787   *vivo* CRISPR-mediated endogenous tagging of Cntn1. DRS, donor recognition sites. AAV were

788   delivered by intracerebroventricular (ICV) injection at P0. **h,** *In vivo* transduction of cortical

789   neurons for CRISPR-dependent genome editing to tag endogenous Cntn1 using smFP-V5 (red).

790   The smFP-V5 tagged Cntn1 colocalizes with β4 spectrin (green) at the AIS (arrowhead). Nuclei

791   are labeled using Hoechst dye (blue). Scale bar, 10 μm.

792
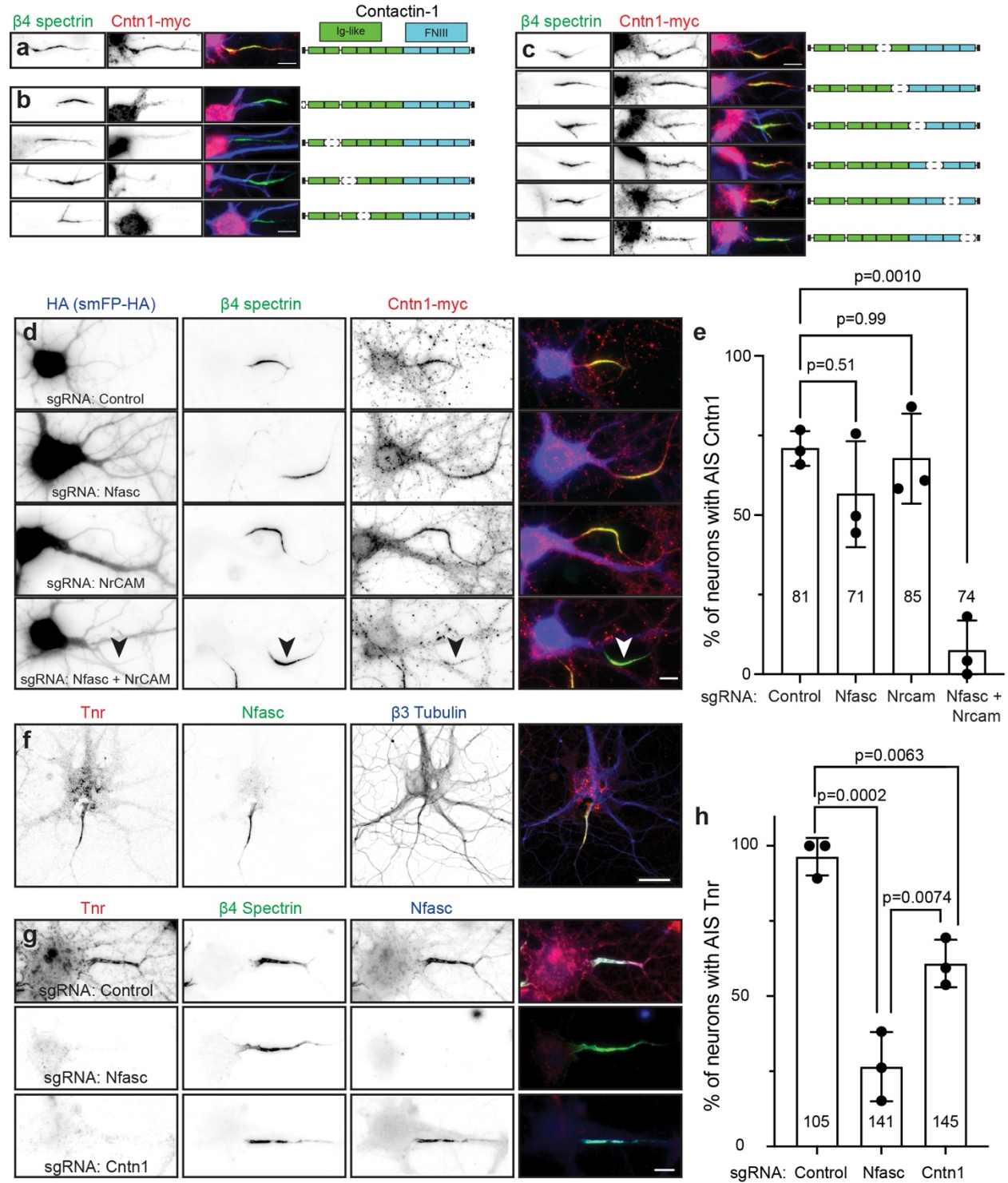
793

794

Ogawa, Lim et al.

795 **Figure 6. Cntn1 is recruited to the AIS through interactions with AnkG-binding L1-family cell**

796 **adhesion molecules. a,** Cntn1-myc (red) is targeted to the AIS and colocalizes with β4 spectrin

797 (green). Cntn1 consists of 6 N-terminal Immunoglobulin (Ig)-like domains and 4 C-terminal

798 Fibronectin type III (FNIII) domains. Scale bar, 10 μm. **b,** Cntn1-myc with N-terminal and

799 internal deletions of the first 4 Ig-like domains fail to localize at the AIS. Scale bar, 10 μm. **c,**

800 Cntn1-myc localization to the AIS does not depend on the last 2 Ig-like domains or any FNIII

801 domain. Scale bar, 10 μm. **d,** Cultured hippocampal neurons transduced with AAV to express

802 Cas9 and control, Nfasc, NrCAM, or Nfasc+NrCAM gRNAs. Neurons were labeled using

803 antibodies against HA as a transduction marker (to label the spaghetti monster fluorescent

804 protein tagged with HA, smFP-HA; blue), β4 spectrin (green), and Cntn1-myc (red). Scale bar,

805 10 μm. **e,** Quantification of the percentage of transduced neurons with AIS Cntn1-myc. N= 3

806 independent experiments. Ordinary one-way ANOVA with Tukey's multiple comparisons test.

807 Error bars, ±SEM. The total number of neurons analyzed is also indicated. **f,** Immunostaining of

808 cultured hippocampal neurons using antibodies against Tenascin R (Tnr; red), β4 spectrin

809 (green), and β3 Tubulin (blue). Scale bar, 25 μm. **g,** Cultured hippocampal neurons transduced

810 with AAV to express Cas9 and control, Nfasc, or Cntn1 gRNAs. Neurons were labeled using

811 antibodies against Tnr (red), β4 spectrin (green), and Nfasc (blue). Scale bar, 10 μm. **h,**

812 Quantification of the percentage of transduced neurons with AIS Tnr. N= 3 independent

813 experiments. Ordinary one-way ANOVA with Tukey's multiple comparisons test. Error bars,

814 ±SEM. The total number of neurons analyzed is also indicated.

815

Ogawa, Lim et al.
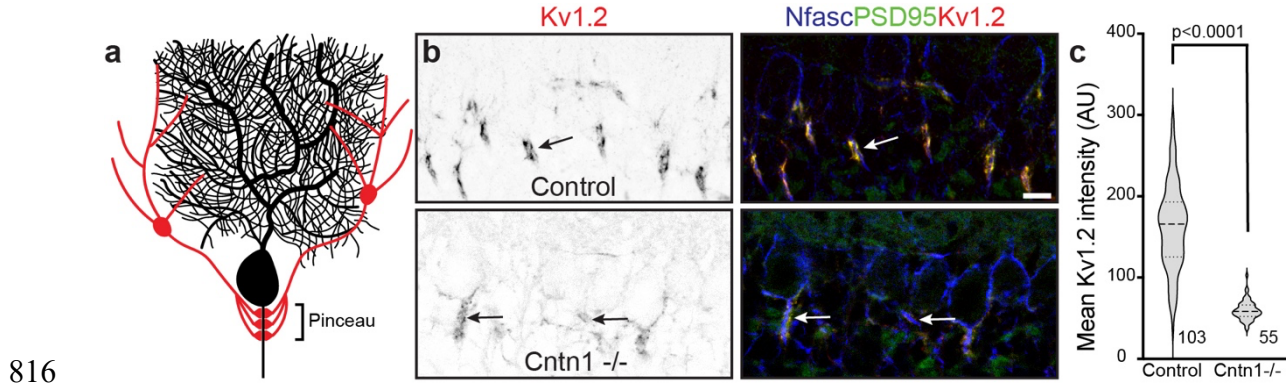
Figure 7. Cntn1 is required for axo-axonic innervation of Purkinje neuron AIS. a, Illustration

of a Purkinje neuron (black) with a basket cell (red) forming the cerebellar pinceau on the AIS.

b, Immunostaining of P17 cerebellar pinceau in control and *Cntn1 -/-* mouse brain using

antibodies against Kv1.2 (red) and PSD95 (green) to label the pinceau, and Nfasc (blue) to label

the Purkinje neuron AIS. Scale bar, 10 µm. **c,** Violin plot of the mean Kv1.2 intensity of the

cerebellar pinceau in control and *Cntn1 -/-* mice. N=3 control and 2 *Cntn1 -/-* mice. The

number of pinceau analyzed is indicated.

Ogawa, Lim et al.

826

827
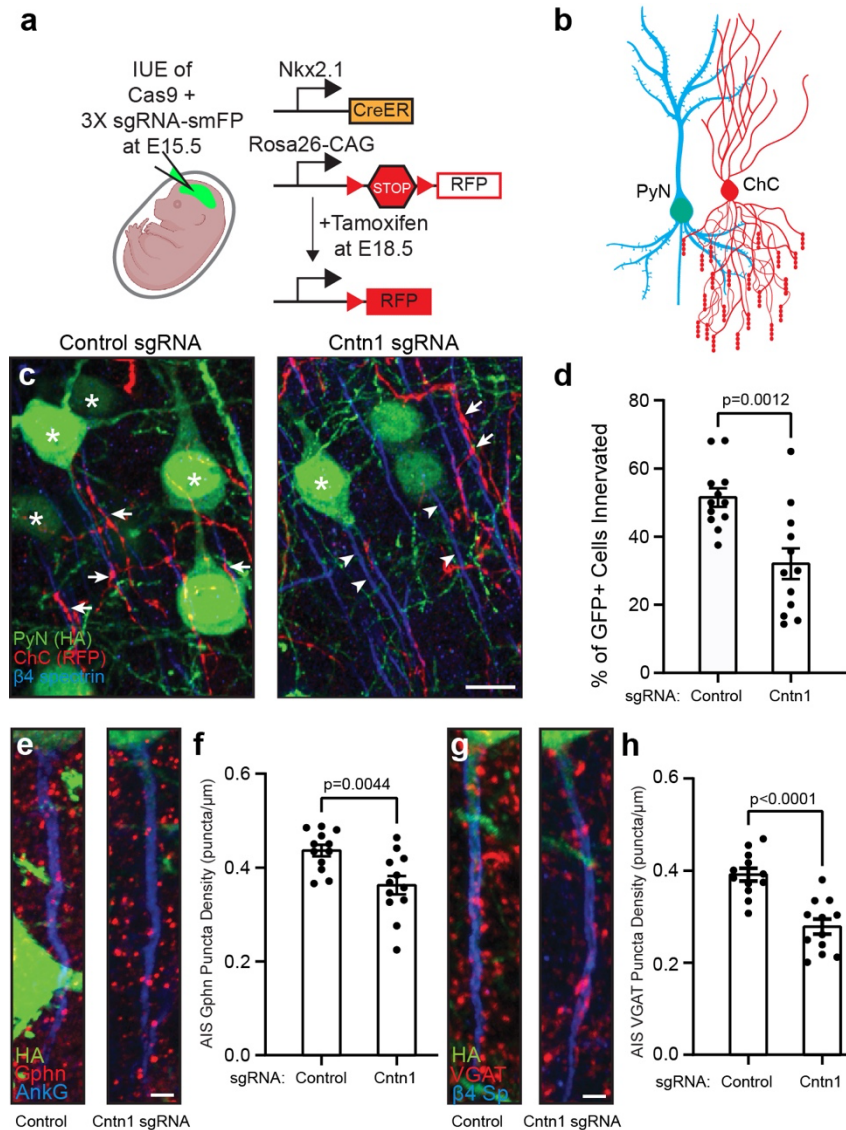
Figure 8. Pyramidal neuron Cntn1 is important for AIS synaptic innervation by ChCs. **a,** Illustration of the knockout and labeling strategy for PyN and ChCs. PyNs are electroporated at E15.5 using plasmids to express Cas9 and 3X sgRNA-smFP (HA tag) to delete expression on Cntn1. ChCs are labeled by expression of red fluorescent protein (RFP) using inducible Cre (CreER) in *Nkx2.1-CreER* mice at E18.5. **b,** Illustration of ChC (red) innervation of PyN (blue/green) AIS. **c,** Representative images of PyNs innervated at their AIS by ChC cartridges (red) in layer II of the

Ogawa, Lim et al.

834   somatosensory cortex from *Nkx2.1-CreER;Ai9 mice* co-electroporated at E15.5 with a plasmid

835   expressing Cas9 and a plasmid expressing smFP-HA and a control sgRNA or Cntn1 sgRNA; mice

836   were sacrificed at P17. AISs and PyNs are visualized by immunostaining for β4 spectrin (blue) and

837   HA (green), respectively. Stars in C indicate HA+ PyNs and arrows indicate ChC innervation of PyN

838   AISs. Arrowheads in C indicate AIS of transfected with Cntn1 sgRNA and that lack innervation by

839   ChC cartridges. Scale bar, 10 μm. **d,** Quantification of the percentage of HA+ PyNs innervated by

840   single RFP+ ChCs at P17. 12 ChCs and 15–66 HA+ PyNs per ChC from 3 animals were analyzed for

841   each condition. Data are mean ± SEM. **e, f,** Representative images of HA+ PyN AISs from *Nkx2.1-*

842   *CreER;Ai9 mice* electroporated at E15.5 with plasmids indicated in (a) and sacrificed at P17.

843   Inhibitory synapses are visualized by immunostaining for the GABAergic postsynaptic marker

844   gephyrin (Gphn; red; **e**) or the GABAergic presynaptic marker VGAT (red; **g**). AISs (blue) are

845   visualized by immunostaining for AnkG in **e** and β4 spectrin in **g**. Scale bars, 2 μm. **f, h,**

846   Quantification of the average number of gephyrin (**f**) or VGAT (**h**) puncta per μm of HA+ PyN AIS

847   at P17. 23-40 AISs from 4 fields of view from 3 animals were analyzed for each condition. Data

848   are mean ± SEM.

849

850

49

Ogawa, Lim et al.

851 **Extended Data:**

852   **1. Supplemental Figures S1-S5**

853   **2. Supplemental extended materials file,** detailed listing of all reagents, plasmids, gRNA

854   sequences, antibodies, sources, etc.

855   **3. Supplemental Table 1,** Nfasc-BAR and NrCAM-BAR proximity proteomes comparison

856   (included as excel file)

857   **4. Supplemental Table 2,** Nfasc-BAR proximity proteomes at DIV 4, 7, 14, 21, and 28

858   (included as excel file).

859   **5. Supplemental Table 3,** Nfasc-BAR fold change and p-values for all identified proteins

860   (included as excel file).

Ogawa, Lim et al.
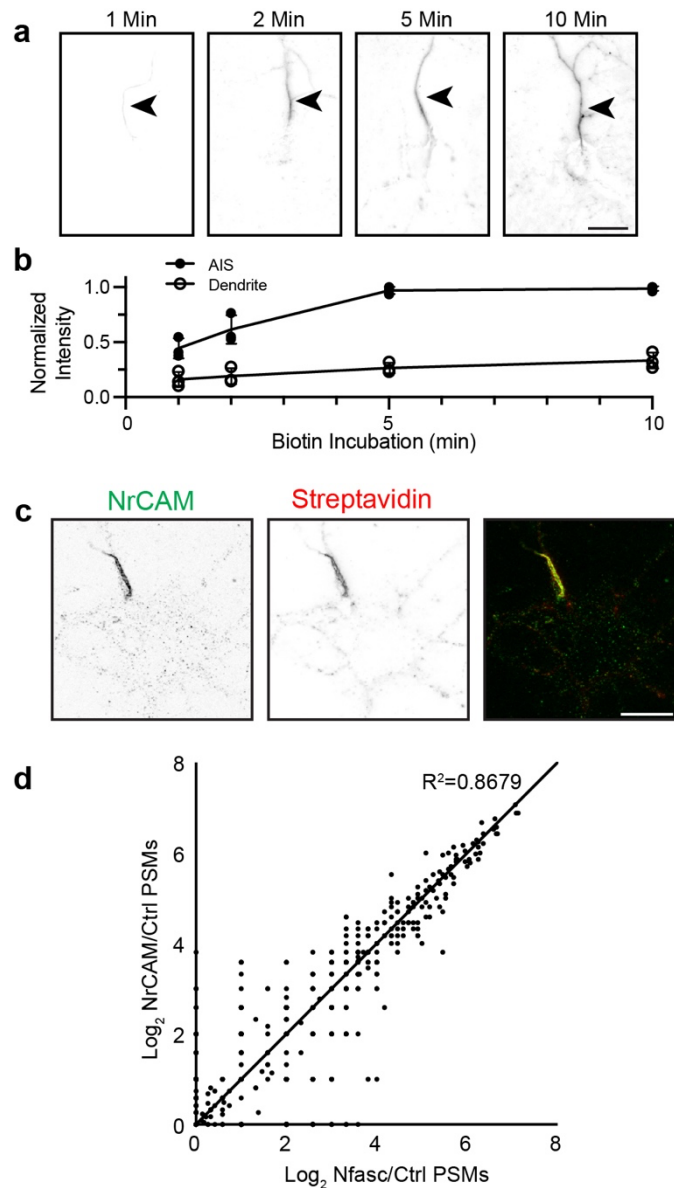
Figure S1. BAR-Nfasc and BAR-NrCAM are highly concordant. a, b, Biotinylation of the AIS

(arrowhead) as a function of biotin-tyramide incubation time. N = 3 independent experiments.

Error bars, ±SEM. Scale bar, 20 μm. **c,** Fluorescence imaging of DIV14 rat hippocampal neurons

labeled by NrCAM-BAR. NrCAM immunofluorescence (green) enrichment defines the AIS.

Biotinylated proteins were detected using Alexa594-conjugated streptavidin. Scale bar, 20 μm.

d, Scatter plot of the number of peptide spectral matches (PSMs) for each biotinylated protein

Ogawa, Lim et al.

868   identified by mass spectrometry using either Nfasc-BAR or NrCAM-BAR. Data were highly

869   concordant since most proteins identified fell on or close to the solid line representing equal

870   enrichment in both BAR conditions.

871

Ogawa, Lim et al.

872
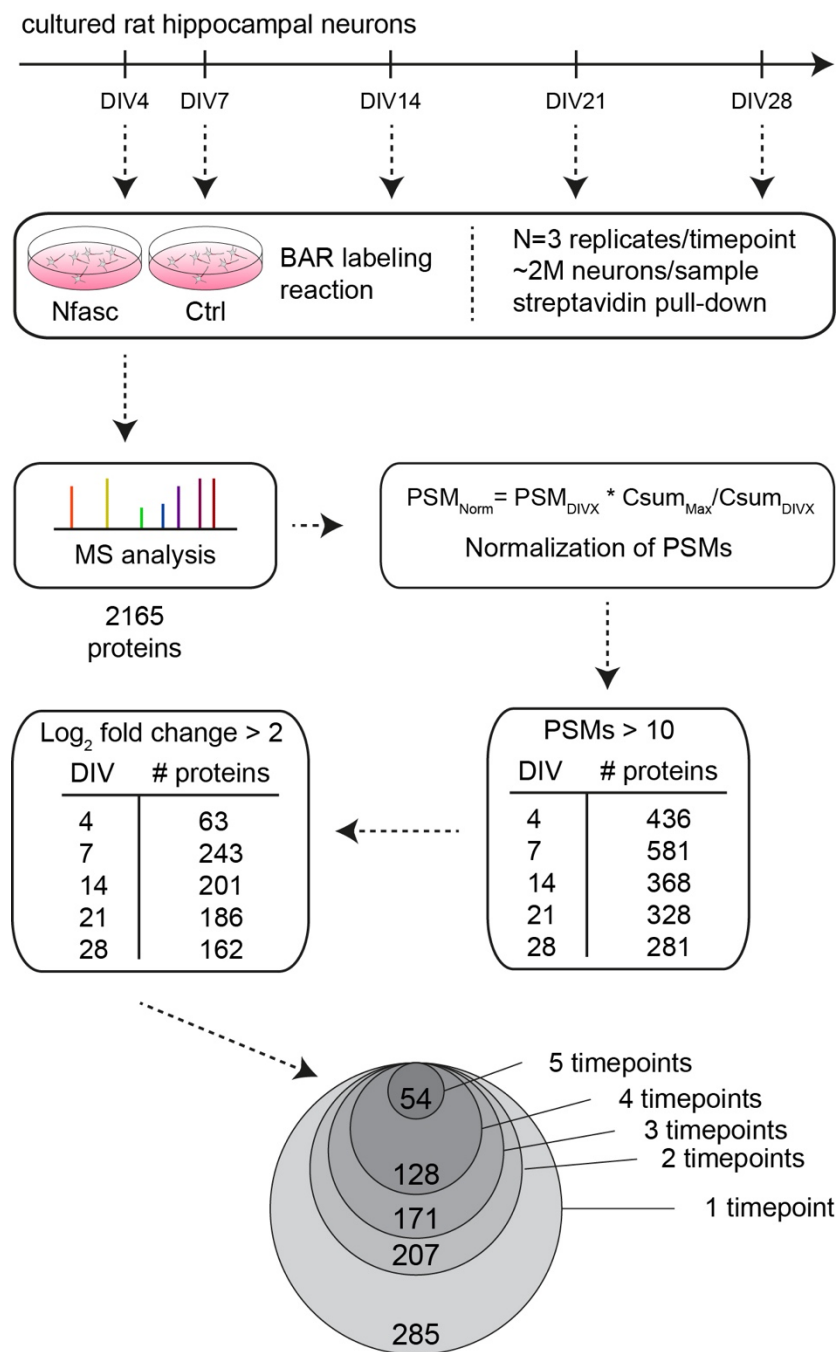
Figure S2. Workflow of Nfasc-BAR labeling and normalization of PSMs. Nfasc-BAR labeling was

performed in triplicate for each of five timepoints. Mass spectrometry analysis resulted in a

dataset of 2165 proteins. To compare across timepoints, PSMs were normalized using the

formula $PSM_{i,}^{Norm,DivX} = PSM_{i,}^{DivX} * SPSM_{Carboxylases}^{DivY} / SPSM_{Carboxylases}^{DivX}$, where i is a particular

53

877   protein on the set, X is a Div time point, Y is the Div time point with the maximum value for

878   summed carboxylase PSMs. Candidates were distinguished from background by filtering based

879   on the number of PSMs identified and the fold change. Tables show the number of proteins

880   that satisfied one or both criteria at a given timepoint. Circles show the number of proteins that

881   satisfied both criteria for 1-5 timepoints.

882

Ogawa, Lim et al.

Ogawa, Lim et al.

884 **Figure S3. Fold-enrichment for the top 100 most enriched proteins identified using Nfasc-BAR**

885 **during *in vitro* neuron development. a-e,** Log$_2$ fold-change (log$_2$(FC)) for the top 100 most

886 enriched proteins identified at DIV 4 (**a**), 7 (**b**), 14 (**c**), 21 (**d**) and 28 (**e**). Known AIS proteins are

887 indicated in red. Error bars, ±SEM.

888

889

Ogawa, Lim et al.
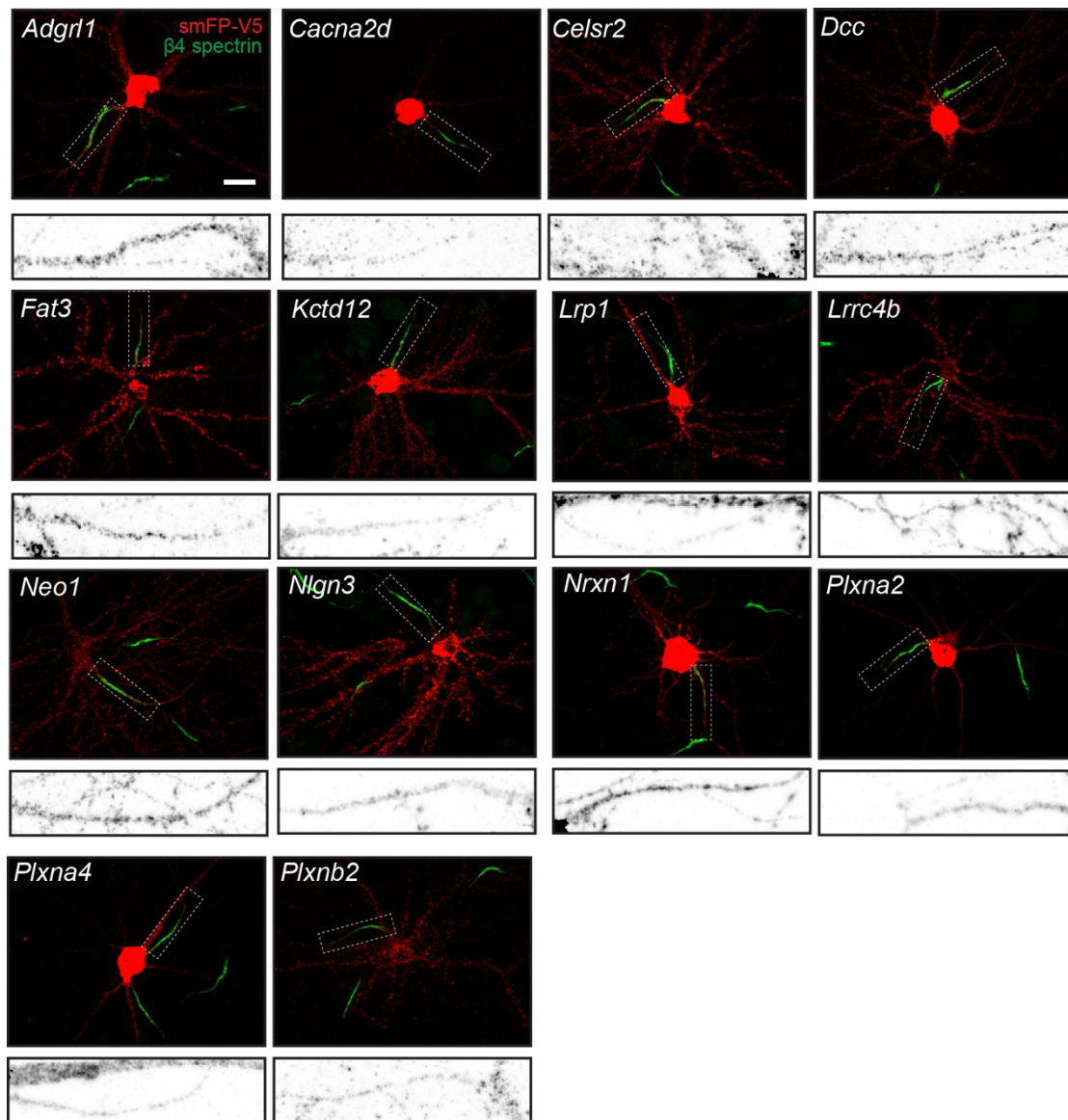
890

891

892   **Figure S4. Tagging of endogenous membrane proteins.** Examples of smFP-V5 tagged

893   proteins (red). AIS are labeled for β4 spectrin (green). The inset boxed regions

894   correspond to the tagged protein at the AIS. Scale bar, 20 μm.

895

896

Ogawa, Lim et al.
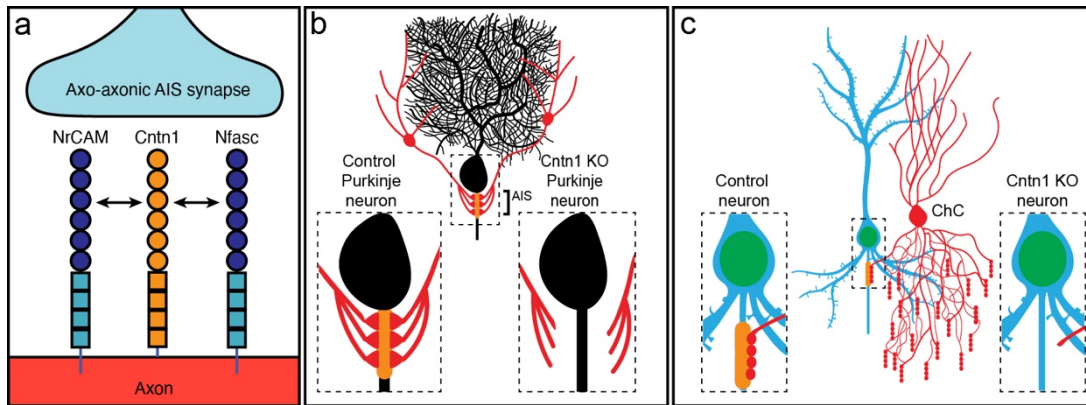
897
898

899   **Figure S5. Summary of results. a,** Cntn1 interacts with and is redundantly recruited to the AIS

900   through interactions with both NrCAM and Nfasc. **b,** Loss of AIS Cntn1 (orange at AIS) from

901   cerebellar Purkinje neurons disrupts basket cell innervation of the AIS and formation of pinceau

902   synapses. **c,** Loss of AIS Cntn1 (orange) from Pyramidal neurons results in reduced innervation

903   of AIS by Chandelier cells (ChC) and reduced numbers of AIS inhibitory synapses.

904

905

Ogawa, Lim et al.

REFERENCES

907 1   Leterrier, C. The Axon Initial Segment: An Updated Viewpoint. *J Neurosci* **38**, 2135-2145,

908   doi:10.1523/JNEUROSCI.1922-17.2018 (2018).

909 2   Rasband, M. N. The axon initial segment and the maintenance of neuronal polarity. *Nat*

910   *Rev Neurosci* **11**, 552-562 (2010).

911 3   Samavarchi-Tehrani, P., Samson, R. & Gingras, A. C. Proximity Dependent Biotinylation:

912   Key Enzymes and Adaptation to Proteomics Approaches. *Molecular & cellular*

913   *proteomics : MCP* **19**, 757-773, doi:10.1074/mcp.R120.001941 (2020).

914 4   Hamdan, H. *et al.* Mapping axon initial segment structure and function by multiplexed

915   proximity biotinylation. *Nature communications* **11**, 100, doi:10.1038/s41467-019-

916   13658-5 (2020).

917 5   Li, J. *et al.* Cell-Surface Proteomic Profiling in the Fly Brain Uncovers Wiring Regulators.

918   *Cell* **180**, 373-386 e315, doi:10.1016/j.cell.2019.12.029 (2020).

919 6   Shuster, S. A. *et al.* In situ cell-type-specific cell-surface proteomic profiling in mice.

920   *Neuron*, doi:10.1016/j.neuron.2022.09.025 (2022).

921 7   Takano, T. *et al.* Chemico-genetic discovery of astrocytic control of inhibition in vivo.

922   *Nature* **588**, 296-302, doi:10.1038/s41586-020-2926-0 (2020).

923 8   Rees, J. S., Li, X. W., Perrett, S., Lilley, K. S. & Jackson, A. P. Selective Proteomic Proximity

924   Labeling Assay Using Tyramide (SPPLAT): A Quantitative Method for the Proteomic

925   Analysis of Localized Membrane-Bound Protein Clusters. *Current protocols in protein*

926   *science / editorial board, John E. Coligan ... [et al.]* **88**, 19.27.11-19.27.18,

927   doi:10.1002/cpps.27 (2017).

59

Ogawa, Lim et al.

928   9   Kotani, N. *et al.* Biochemical visualization of cell surface molecular clustering in living

929   cells. *Proc Natl Acad Sci U S A* **105**, 7405-7409, doi:10.1073/pnas.0710346105 (2008).

930   10   Bar, D. Z. *et al.* Biotinylation by antibody recognition-a method for proximity labeling.

931   *Nature methods* **15**, 127-133, doi:10.1038/nmeth.4533 (2018).

932   11   Oakley, J. V. *et al.* Radius measurement via super-resolution microscopy enables the

933   development of a variable radii proximity labeling platform. *Proc Natl Acad Sci U S A*

934   **119**, e2203027119, doi:10.1073/pnas.2203027119 (2022).

935   12   Amor, V. *et al.* The paranodal cytoskeleton clusters Na(+) channels at nodes of Ranvier.

936   *eLife* **6**, doi:10.7554/eLife.21392 (2017).

937   13   Ghosh, A., Malavasi, E. L., Sherman, D. L. & Brophy, P. J. Neurofascin and Kv7.3 are

938   delivered to somatic and axon terminal surface membranes en route to the axon initial

939   segment. *eLife* **9**, doi:10.7554/eLife.60619 (2020).

940   14   Yang, Y., Ogawa, Y., Hedstrom, K. L. & Rasband, M. N. βIV spectrin is recruited to axon

941   initial segments and nodes of Ranvier by ankyrinG. *J Cell Biol* **176**, 509-519 (2007).

942   15   Hedstrom, K. L. *et al.* Neurofascin assembles a specialized extracellular matrix at the

943   axon initial segment. *J Cell Biol* **178**, 875-886, doi:10.1083/jcb.200705119 (2007).

944   16   Stevens, S. R. *et al.* Ankyrin-R regulates fast-spiking interneuron excitability through

945   perineuronal nets and Kv3.1b K(+) channels. *eLife* **10**, doi:10.7554/eLife.66491 (2021).

946   17   Pollerberg, G. E., Thelen, K., Theiss, M. O. & Hochlehnert, B. C. The role of cell adhesion

947   molecules for navigating axons: density matters. *Mech Dev* **130**, 359-372,

948   doi:10.1016/j.mod.2012.11.002 (2013).

Ogawa, Lim et al.

949   18   Buffington, S. A., Sobotzik, J. M., Schultz, C. & Rasband, M. N. IkappaBalpha is not

950   required for axon initial segment assembly. *Mol Cell Neurosci* **50**, 1-9,

951   doi:10.1016/j.mcn.2012.03.003 (2012).

952   19   Ogawa, Y. & Rasband, M. N. Endogenously expressed Ranbp2 is not at the axon initial

953   segment. *J Cell Sci* **134**, doi:10.1242/jcs.256180 (2021).

954   20   Chang, K. J., Susuki, K., Dours-Zimmermann, M. T., Zimmermann, D. R. & Rasband, M. N.

955   Oligodendrocyte myelin glycoprotein does not influence node of ranvier structure or

956   assembly. *J Neurosci* **30**, 14476-14481 (2010).

957   21   Suzuki, K. *et al.* In vivo genome editing via CRISPR/Cas9 mediated homology-

958   independent targeted integration. *Nature* **540**, 144-149, doi:10.1038/nature20565

959   (2016).

960   22   Gao, Y. *et al.* Plug-and-Play Protein Modification Using Homology-Independent Universal

961   Genome Engineering. *Neuron*, doi:10.1016/j.neuron.2019.05.047 (2019).

962   23   Willems, J. *et al.* ORANGE: A CRISPR/Cas9-based genome editing toolbox for epitope

963   tagging of endogenous proteins in neurons. *PLoS Biol* **18**, e3000665,

964   doi:10.1371/journal.pbio.3000665 (2020).

965   24   Davis, J. Q. & Bennett, V. Ankyrin binding activity shared by the neurofascin/L1/NrCAM

966   family of nervous system cell adhesion molecules. *J Biol Chem* **269**, 27163-27166 (1994).

967   25   Boiko, T. *et al.* Ankyrin-dependent and -independent mechanisms orchestrate axonal

968   compartmentalization of L1 family members neurofascin and L1/neuron-glia cell

969   adhesion molecule. *J Neurosci* **27**, 590-603 (2007).

Ogawa, Lim et al.

970   26   Pinatel, D. *et al.* The Kv1-associated molecules TAG-1 and Caspr2 are selectively

971   targeted to the axon initial segment in hippocampal neurons. *J Cell Sci* **130**, 2209-2220,

972   doi:10.1242/jcs.202267 (2017).

973   27   Davis, J. Q., Lambert, S. & Bennett, V. Molecular composition of the node of Ranvier:

974   identification of ankyrin-binding cell adhesion molecules neurofascin (mucin+/third FNIII

975   domain-) and NrCAM at nodal axon segments. *J Cell Biol* **135**, 1355-1367 (1996).

976   28   Shimoda, Y. & Watanabe, K. Contactins: emerging key roles in the development and

977   function of the nervous system. *Cell Adh Migr* **3**, 64-70, doi:10.4161/cam.3.1.7764

978   (2009).

979   29   Charles, P. *et al.* Neurofascin is a glial receptor for the paranodin/Caspr-contactin axonal

980   complex at the axoglial junction. *Curr Biol* **12**, 217-220. (2002).

981   30   Boyle, M. E. *et al.* Contactin orchestrates assembly of the septate-like junctions at the

982   paranode in myelinated peripheral nerve. *Neuron* **30**, 385-397. (2001).

983   31   Rios, J. C. *et al.* Contactin-associated protein (Caspr) and contactin form a complex that

984   is targeted to the paranodal junctions during myelination. *J Neurosci* **20**, 8354-8364.

985   (2000).

986   32   Colakoglu, G., Bergstrom-Tyrberg, U., Berglund, E. O. & Ranscht, B. Contactin-1 regulates

987   myelination and nodal/paranodal domain organization in the central nervous system.

988   *Proc Natl Acad Sci U S A* **111**, E394-403, doi:10.1073/pnas.1313769110 (2014).

989   33   Volkmer, H., Zacharias, U., Norenberg, U. & Rathjen, F. G. Dissection of complex

990   molecular interactions of neurofascin with axonin-1, F11, and tenascin-R, which

Ogawa, Lim et al.

991   promote attachment and neurite formation of tectal cells. *J Cell Biol* **142**, 1083-1093

992   (1998).

993 34   Gollan, L., Salomon, D., Salzer, J. L. & Peles, E. Caspr regulates the processing of

994   contactin and inhibits its binding to neurofascin. *J Cell Biol* **163**, 1213-1218 (2003).

995 35   Kole, M. J. *et al.* Selective Loss of Presynaptic Potassium Channel Clusters at the

996   Cerebellar Basket Cell Terminal Pinceau in Adam11 Mutants Reveals Their Role in

997   Ephaptic Control of Purkinje Cell Firing. *J Neurosci* **35**, 11433-11444,

998   doi:10.1523/JNEUROSCI.1346-15.2015 (2015).

999 36   Laube, G. *et al.* Ultrastructural localization of Shaker-related potassium channel subunits

1000   and synapse-associated protein 90 to septate-like junctions in rat cerebellar Pinceaux.

1001   *Brain Res Mol Brain Res* **42**, 51-61 (1996).

1002 37   Ango, F. *et al.* Ankyrin-based subcellular gradient of neurofascin, an immunoglobulin

1003   family protein, directs GABAergic innervation at purkinje axon initial segment. *Cell* **119**,

1004   257-272 (2004).

1005 38   Dudok, B. *et al.* Recruitment and inhibitory action of hippocampal axo-axonic cells

1006   during behavior. *Neuron* **109**, 3838-3850 e3838, doi:10.1016/j.neuron.2021.09.033

1007   (2021).

1008 39   Schneider-Mizell, C. M. *et al.* Structure and function of axo-axonic inhibition. *eLife* **10**,

1009   doi:10.7554/eLife.73783 (2021).

1010 40   Gallo, N. B., Paul, A. & Van Aelst, L. Shedding Light on Chandelier Cell Development,

1011   Connectivity, and Contribution to Neural Disorders. *Trends Neurosci* **43**, 565-580,

1012   doi:10.1016/j.tins.2020.05.003 (2020).

Ogawa, Lim et al.

1013   41   Tai, Y., Gallo, N. B., Wang, M., Yu, J. R. & Van Aelst, L. Axo-axonic Innervation of

1014   Neocortical Pyramidal Neurons by GABAergic Chandelier Cells Requires AnkyrinG-

1015   Associated L1CAM. *Neuron*, doi:10.1016/j.neuron.2019.02.009 (2019).

1016   42   Zhou, D. *et al.* AnkyrinG is required for clustering of voltage-gated Na channels at axon

1017   initial segments and for normal action potential firing. *J Cell Biol* **143**, 1295-1304 (1998).

1018   43   Hedstrom, K. L., Ogawa, Y. & Rasband, M. N. AnkyrinG is required for maintenance of

1019   the axon initial segment and neuronal polarity. *J Cell Biol* **183**, 635-640,

1020   doi:10.1083/jcb.200806112 (2008).

1021   44   Torii, T. *et al.* NuMA1 promotes axon initial segment assembly through inhibition of

1022   endocytosis. *J Cell Biol* **219**, doi:10.1083/jcb.201907048 (2020).

1023   45   Peles, E. *et al.* Identification of a novel contactin-associated transmembrane receptor

1024   with multiple domains implicated in protein-protein interactions. *EMBO J* **16**, 978-988

1025   (1997).

1026   46   Zisch, A. H. *et al.* Neuronal cell adhesion molecule contactin/F11 binds to tenascin via its

1027   immunoglobulin-like domains. *J Cell Biol* **119**, 203-213, doi:10.1083/jcb.119.1.203

1028   (1992).

1029   47   Peles, E. *et al.* The carbonic anhydrase domain of receptor tyrosine phosphatase beta is

1030   a functional ligand for the axonal cell recognition molecule contactin. *Cell* **82**, 251-260

1031   (1995).

1032   48   Kazarinova-Noyes, K. *et al.* Contactin associates with Na+ channels and increases their

1033   functional expression. *J Neurosci* **21**, 7517-7525. (2001).

Ogawa, Lim et al.

1034 49 Reischer, T., Liebmann-Reindl, S., Bettelheim, D., Balendran-Braun, S. & Streubel, B.

1035   Genetic diagnosis and clinical evaluation of severe fetal akinesia syndrome. *Prenat*

1036   *Diagn* **40**, 1532-1539, doi:10.1002/pd.5809 (2020).

1037 50 Blot, A. & Barbour, B. Ultra-rapid axon-axon ephaptic inhibition of cerebellar Purkinje

1038   cells by the pinceau. *Nat Neurosci* **17**, 289-295, doi:10.1038/nn.3624 (2014).

1039 51 Jenkins, S. M. & Bennett, V. Ankyrin-G coordinates assembly of the spectrin-based

1040   membrane skeleton, voltage-gated sodium channels, and L1 CAMs at Purkinje neuron

1041   initial segments. *J Cell Biol* **155**, 739-746. (2001).

1042 52 Zonta, B. *et al.* A Critical Role for Neurofascin in Regulating Action Potential Initiation

1043   through Maintenance of the Axon Initial Segment. *Neuron* **69**, 945-956 (2011).

1044 53 Hayano, Y. *et al.* IgSF11 homophilic adhesion proteins promote layer-specific synaptic

1045   assembly of the cortical interneuron subtype. *Sci Adv* **7**, doi:10.1126/sciadv.abf1600

1046   (2021).

1047 54 Cho, K. F. *et al.* Split-TurboID enables contact-dependent proximity labeling in cells. *Proc*

1048   *Natl Acad Sci U S A* **117**, 12143-12154, doi:10.1073/pnas.1919528117 (2020).

1049 55 Taniguchi, H., Lu, J. & Huang, Z. J. The spatial and temporal origin of chandelier cells in

1050   mouse neocortex. *Science* **339**, 70-74, doi:10.1126/science.1227622 (2013).

1051 56 Guan, S., Price, J. C., Prusiner, S. B., Ghaemmaghami, S. & Burlingame, A. L. A data

1052   processing pipeline for mammalian proteome dynamics studies using stable isotope

1053   metabolic labeling. *Molecular & cellular proteomics : MCP* **10**, M111 010728,

1054   doi:10.1074/mcp.M111.010728 (2011).

Ogawa, Lim et al.

1055   57   Clauser, K. R., Baker, P. & Burlingame, A. L. Role of accurate mass measurement (+/- 10

1056   ppm) in protein identification strategies employing MS or MS/MS and database

1057   searching. *Anal Chem* **71**, 2871-2882 (1999).

1058   58   Suzuki, K. & Izpisua Belmonte, J. C. In vivo genome editing via the HITI method as a tool

1059   for gene therapy. *Journal of human genetics* **63**, 157-164, doi:10.1038/s10038-017-

1060   0352-4 (2018).

1061   59   Konno, A. & Hirai, H. Efficient whole brain transduction by systemic infusion of

1062   minimally purified AAV-PHP.eB. *J Neurosci Methods* **346**, 108914,

1063   doi:10.1016/j.jneumeth.2020.108914 (2020).

1064   60   Kim, J. Y., Grunke, S. D., Levites, Y., Golde, T. E. & Jankowsky, J. L.

1065   Intracerebroventricular viral injection of the neonatal mouse brain for persistent and

1066   widespread neuronal transduction. *J Vis Exp*, 51863, doi:10.3791/51863 (2014).

1067